Genomics Proteomics Bioinformatics 21 (2023) 707–728

Genomics Proteomics Bioinformatics

www.elsevier.com/locate/gpb
www.sciencedirect.com

ORIGINAL RESEARCH

Specific Regulation of m^{6}A by SRSF7 Promotes the Progression of Glioblastoma

Yixian Cun [1,2,#], Sanqi An [3,4,5,#], Haiqing Zheng [1,#], Jing Lan [6], Wenfang Chen [3,4], Wanjun Luo [6], Chengguo Yao [4], Xincheng Li [1,2], Xiang Huang [3,4], Xiang Sun [3,4], Zehong Wu [3,4], Yameng Hu [1,2], Ziwen Li [1,2], Shuxia Zhang [1,2], Geyan Wu [7], Meisongzhu Yang [1,2], Miaoling Tang [7], Ruyuan Yu [1,2], Xinyi Liao [1,2], Guicheng Gao [3,4], Wei Zhao [4], Jinkai Wang [3,4,8,*], Jun Li [1,2,*]

[1] *Department of Rehabilitation Medicine, Key Laboratory of Liver Disease of Guangdong Province, The Third Affiliated Hospital, Sun Yat-sen University, Guangzhou 510080, China*
[2] *Department of Biochemistry, Zhongshan School of Medicine, Sun Yat-sen University, Guangzhou 510080, China*
[3] *Department of Medical Informatics, Zhongshan School of Medicine, Sun Yat-sen University, Guangzhou 510080, China*
[4] *Center for Stem Cell Biology and Tissue Engineering, Key Laboratory for Stem Cells and Tissue Engineering, Ministry of Education, Sun Yat-sen University, Guangzhou 510080, China*
[5] *Biosafety Level-3 Laboratory, Life Sciences Institute, Guangxi Medical University, Nanning 530020, China*
[6] *Department of Obstetrics and Gynecology, The First Affiliated Hospital, Sun Yat-sen University, Guangzhou 510080, China*
[7] *State Key Laboratory of Oncology in South China, Cancer Center, Sun Yat-sen University, Guangzhou 510080, China*
[8] *RNA Biomedical Institute, Sun Yat-sen Memorial Hospital, Sun Yat-sen University, Guangzhou 510080, China*

Received 24 August 2021; revised 6 November 2021; accepted 14 December 2021
Available online 23 December 2021

Handled by Chengqi Yi

KEYWORDS

m^{6}A;
Serine/arginine-rich splicing factor 7;
Cell-specific regulation;
Glioblastoma;
PDZ-binding kinase

Abstract **Serine/arginine-rich splicing factor 7** (SRSF7), a known splicing factor, has been revealed to play oncogenic roles in multiple cancers. However, the mechanisms underlying its oncogenic roles have not been well addressed. Here, based on N^6-methyladenosine (**m^{6}A**) co-methylation network analysis across diverse cell lines, we find that the gene expression of *SRSF7* is positively correlated with **glioblastoma** (GBM) cell-specific m^{6}A methylation. We then indicate that SRSF7 is a novel m^{6}A regulator, which specifically facilitates the m^{6}A methylation near its binding sites on the mRNAs involved in cell proliferation and migration, through recruiting the methyltransferase complex. Moreover, SRSF7 promotes the proliferation and migration of GBM cells largely dependent on the presence of the m^{6}A methyltransferase. The two m^{6}A sites on the mRNA for **PDZ-binding kinase**

* Corresponding authors.
E-mail: lijun37@mail.sysu.edu.cn (Li J), wangjk@mail.sysu.edu.cn (Wang J).
# Equal contribution.

Peer review under responsibility of Beijing Institute of Genomics, Chinese Academy of Sciences / China National Center for Bioinformation and Genetics Society of China.

https://doi.org/10.1016/j.gpb.2021.11.001

(*PBK*) are regulated by SRSF7 and partially mediate the effects of SRSF7 in GBM cells through recognition by insulin-like growth factor 2 mRNA-binding protein 2 (IGF2BP2). Together, our discovery reveals a novel role of SRSF7 in regulating m^{6}A and validates the presence and functional importance of temporal- and spatial-specific regulation of m^{6}A mediated by RNA-binding proteins (RBPs).

Introduction

Serine/arginine-rich splicing factor 7 (SRSF7, also known as 9G8) belongs to the serine/arginine (SR) protein family, which contains 7 canonical members (SRSF1–7) [1]. It is previously known as a splicing factor to regulate alternative splicing as well as a regulator of alternative polyadenylation (APA) [2–5]. SRSF7 is also an adaptor of nuclear RNA export factor (NXF1), which exports mature RNAs out of nucleus, and plays important roles in coupling RNA alternative splicing and APA to mRNA export [5]. It has been reported that hyperphosphorylated SRSF7 binds to pre-mRNA for splicing and SRSF7 becomes hypophosphorylated during splicing, and the later form of SRSF7 can bind to NXF1 for the subsequent export of the spliced RNAs [3].

The oncogenic roles of SRSF7 have been widely reported. It was discovered as a critical gene required for cell growth or viability in multiple cancer cell lines based on a genome-wide CRISPR/Cas9 screening [6]. Aberrantly elevated expression of *SRSF7* was observed in lung cancer, colon cancer, and gastric cancer [7–9]. It was also reported to be highly expressed in glioblastoma [GBM, world health organization (WHO) grade IV glioma] and associated with poor patient outcome [10]. However, although SRSF7 has been reported to regulate splicing, APA, and mRNA export, the mechanisms underlying its oncogenic roles have not been well addressed.

N^6-methyladenosine (m^{6}A) is a reversible RNA modification prevalent in eukaryotic mRNAs and long non-coding RNAs [11–14]. It plays critical roles in various biological processes, including stem cell differentiation, immune system, learning and memory, and cancer development [15–20]. m^{6}A modification is marked by the m^{6}A methyltransferase (also known as "writer") complex, which consists of methyltransferase-like 3 (METTL3), methyltransferase-like 14 (METTL14), Wilms tumor 1-associating protein (WTAP), vir-like m^{6}A methyltransferase associated (VIRMA), zinc finger CCCH-type containing 13 (ZC3H13), RNA-binding motif protein 15/15B (RBM15/15B), and cbl proto-oncogene like 1 (CBLL1, also known as HAKAI) [21–23]. m^{6}A can also be removed by demethylases (also known as "erasers") including fat mass and obesity associated gene (FTO) and alkB homolog 5 (ALKBH5) [24,25]. The m^{6}A-modified RNAs are recognized by a series of readers such as YTH-domain containing proteins (YTHDF1–3 and YTHDC1–2) [26]. For instance, YTHDF 2 facilitates the degradation of methylated RNAs and is important for cell fate transitions [27–30]. Insulin-like growth factor 2 mRNA-binding protein 1–3 (IGF2BP1–3) are a different type of readers that can stabilize the methylated RNAs and play oncogenic roles in multiple types of cancers [31]. In addition, m^{6}A can also down-regulate gene expression through degrading chromosome-associated regulatory RNAs (carRNAs) [32] and up-regulate gene expression by demethylating H3K9me2 histone modification [33].

Unlike global regulation of m^{6}A by the methyltransferase complex, selective modification of m^{6}A on specific targets can shape the cell-specific methylome and mediate specific functions in diverse biological systems. There are different mechanisms that confer the specificities of m^{6}A. Although the components of methyltransferase complex VIRMA and ZC3H13 mainly affect the m^{6}A at stop codons and 3′ untranslated regions (3′ UTRs), their substantial effects on m^{6}A suggest fundamental but limited specificities for m^{6}A installation, consistent with that they do not have RNA-binding domain and ZC3H13 works to take the methyltransferase into nucleus [34,35]. Since m^{6}A occurs co-transcriptionally, m^{6}A could be specifically regulated co-transcriptionally through H3K36me3 and transcription factors. Depletion of H3K36me3 also results in global reduction of m^{6}A, especially the m^{6}A at 3′ UTRs and protein-coding regions, suggesting a fundamental but relatively low specificity in regulation of m^{6}A [36]. On the other hand, transcription factors CCAAT/enhancer-binding protein zeta (CEBPZ) and sma- and mad-related protein (SMAD) family member 2/3 (SMAD2/3) can recruit the methyltransferase to methylate the nascent RNAs being transcribed by them and play important roles in acute myeloid leukemia oncogenesis and stem cell differentiation, respectively [37]. The specificities of transcription factors are conferred by their binding specificities on the promoters. Therefore, they can mediate highly specific methylation other than global regulation of m^{6}A. However, transcription factors usually bind at the 5′ end, and thus cannot precisely direct the m^{6}A modification at specific loci of the RNAs. In contrast to transcription factors, which select RNAs other than sites, RNA-binding proteins (RBPs) have the potential to precisely guide the methylation at specific sites of RNAs in the similar manner as they regulate alternative splicing [38]. Recently, we developed a co-methylation network based computational framework and revealed a large number of RBPs acting as m^{6}A *trans*-regulators to specifically regulate m^{6}A to form cell-specific m^{6}A methylomes [39]. However, firm experimental validations and profound characterizations are still lacking, and whether these RBPs play important functional roles through regulating the m^{6}A of specific sites is not clear either.

In this study, we find that SRSF7 specifically regulates m^{6}A on the genes involved in cell proliferation and migration, and plays oncogenic roles through recruiting the m^{6}A methyltransferase complex near its binding sites in GBM cells. Our discovery reveals a novel role of SRSF7 in regulating m^{6}A and timely confirms the existence and importance of RBP-mediated temporal- and spatial-specific regulation of m^{6}A.

Results

SRSF7 is a potential m^{6}A regulator that interacts with m^{6}A methyltransferase complex

To elucidate how cells establish cell-specific m^{6}A methylomes, we previously developed a co-methylation network based computational framework to systematically identify the

cell-specific *trans*-regulators of m^{6}A [39]. We first identified the RBPs with gene expression correlated with the m^{6}A ratio (level) of specific co-methylation module (a subset of co-methylated m^{6}A peaks) across 25 different cell lines (the detailed information of cell lines can be found in the supplementary table of [39]). By further investigating the enrichment of binding targets of the RBPs within their correlated modules based on cross-linking and immunoprecipitation combined with high throughput sequencing (CLIP-seq) data of 157 RBPs and motifs of 89 RBPs, we revealed widespread cell-specific *trans*-regulation of m^{6}A and predicted 32 high-confidence m^{6}A regulators [39]. It is of great importance to understand whether these RBP-mediated specific regulations of m^{6}A play critical functional roles. This co-methylation network provides the information about cell specificities of different modules, which gives valuable clues for us to speculate the functions of these modules. We realized that one of the modules (M5) was highly methylated in two GBM cell lines (PBT003 and GSC) (**Figure 1**A). Coincidently, although not significant enough to bear multiple testing correction, the mostly enriched Gene Ontology (GO) terms for the corresponding genes of this module were glioma- and cancer-related pathways (Figure 1B), suggesting that the specific methylation of this module may play a role in the development of glioma. We then tried to dissect the RBPs that direct the specific m^{6}A methylation of this glioma-related module. As we have previously determined [39] and shown at the bottom of Figure 1A, there were 6 RBPs with gene expression significantly correlated with the m^{6}A index (the first component of principal component analysis) of module M5, including 2 positive and 4 negative correlations. We further analyzed the prognostic relevance of these 6 RBPs in GBM patients from Chinese Glioma Genome Atlas (CGGA) dataset [40]. We found that the expression of *SRSF7* was most significantly correlated with the survival time of GBM patients (Figure 1C). Highly expression of *SRSF7* was associated with highly m^{6}A methylation of the m^{6}A sites in this module and poor prognosis of the GBM patients (Figure 1D and E). Although the other 5 RBPs may also regulate m^{6}A of this module in GBM cells, they cannot really affect the prognosis of GBM patients, we therefore focused on SRSF7 to investigate whether and how it plays important roles in GBM through specific regulation of m^{6}A.

To test whether SRSF7 is a genuine m^{6}A regulator that facilitates the installation of m^{6}A at specific m^{6}A sties, we first examined whether SRSF7 can interact with the core m^{6}A methyltransferase complex composed of METTL3, METTL14, and WTAP in a GBM cell line U87MG. Co-immunoprecipitation (Co-IP) assays revealed that Flag-tagged SRSF7 could pull down the endogenous METTL3, METTL14, and WTAP independent of RNA (Figure 1F and G). Reciprocally, both Flag-tagged METTL3 and WTAP could also pull down endogenous SRSF7 in an RNA-independent manner, respectively, in U87MG cells (Figure 1H and I). Similar results were observed in 293 T cells (Figure S1A), suggesting that the interaction between SRSF7 and the methyltransferase complex is a universal mechanism. In addition, we performed Co-IP using truncated SRSF7 with RNA recognition motif (RRM) domain or arginine/serine (RS) domain deleted in U87MG cells, and found that deletion of RRM domain other than RS domain could disrupt the interactions with METTL3, METTL14, and WTAP (Figure 1J, Figure S1B), indicating that SRSF7 interacts with the methyltransferase complex through its RRM domain.

We then used 3D structured illumination microscopy (3D-SIM) super-resolution microscopy to test the protein colocalization between SRSF7 and the m^{6}A methyltransferase complex in U87MG cells. We found that a portion of SRSF7 proteins were colocalized with portions of METTL3, METTL14, and WTAP in the nucleus, respectively (Figure 1K), implying that at least a part of SRSF7 proteins can specifically regulate m^{6}A. The aforementioned results suggest that SRSF7 may be able to regulate m^{6}A through recruiting the m^{6}A methyltransferase complex.

SRSF7 specifically facilitates m^{6}A modification near its binding sites

To further investigate whether SRSF7 regulates m^{6}A modification, we knocked down *SRSF7* and performed m^{6}A-seq to examine the m^{6}A alteration due to *SRSF7* depletion in U87MG cells. The typical m^{6}A motif was enriched in the m^{6}A peaks of both knockdown and control cells (Figure S2A). As shown in Figure S2B, the m^{6}A peaks were enriched near the stop codons in both knockdown and control cells, which is consistent with previous studies [11,12]. In contrast to the RBPs in the m^{6}A methyltransferase complex, which usually cause massive loss of m^{6}A upon depletion [22], depletion of *SRSF7* did not alter the distribution (Figure S2B) and overall peak intensities of the m^{6}A peaks (Figure S2C), suggesting that SRSF7 may be a different type of m^{6}A regulator that regulates a small number of highly specific m^{6}A sites in U87MG cells.

We then determined the differentially methylated m^{6}A sites between *SRSF7* knockdown and control to understand the specific sites regulated by SRSF7. After *SRSF7* knockdown, 3334 m^{6}A peaks in 2440 genes were down-regulated; in contrast, only 2447 peaks in 1850 genes were up-regulated (**Figure 2**A, Figure S2D). GO analysis and Kyoto Encyclopedia of Genes and Genomes (KEGG) analysis showed that these differentially methylated genes were enriched in terms including cell division, cell migration, cell proliferation, and pathway in cancer (Figure S2E and F).

To further confirm that SRSF7 regulates the m^{6}A sites through binding near the m^{6}A sites, we performed individual-nucleotide resolution UV crosslinking and immunoprecipitation combined with high throughput sequencing (iCLIP-seq) [41] for SRSF7 to identify the transcriptome-wide binding sites of SRSF7 in U87MG cells. We identified 40,476 iCLIP-seq peaks using CLIP Tool Kit (CTK) [42] (Table S1). The enriched motifs were similar as the previously reported motif of SRSF7 (GAYGAY) [43] (Figure 2B), suggesting the high reliability of our iCLIP-seq data. Interestingly, the m^{6}A motif was also enriched in the SRSF7 iCLIP-seq peaks (Figure 2B), suggesting the colocalization of SRSF7 with m^{6}A sites. We found that only 7.9% and 3.1% of the peaks were in introns and non-coding RNAs, respectively; in contrast, 66.8% of the peaks were in protein-coding regions, which are similar as the distribution of m^{6}A (Figure S2G). However, the peaks were more enriched at the 5′ end of the

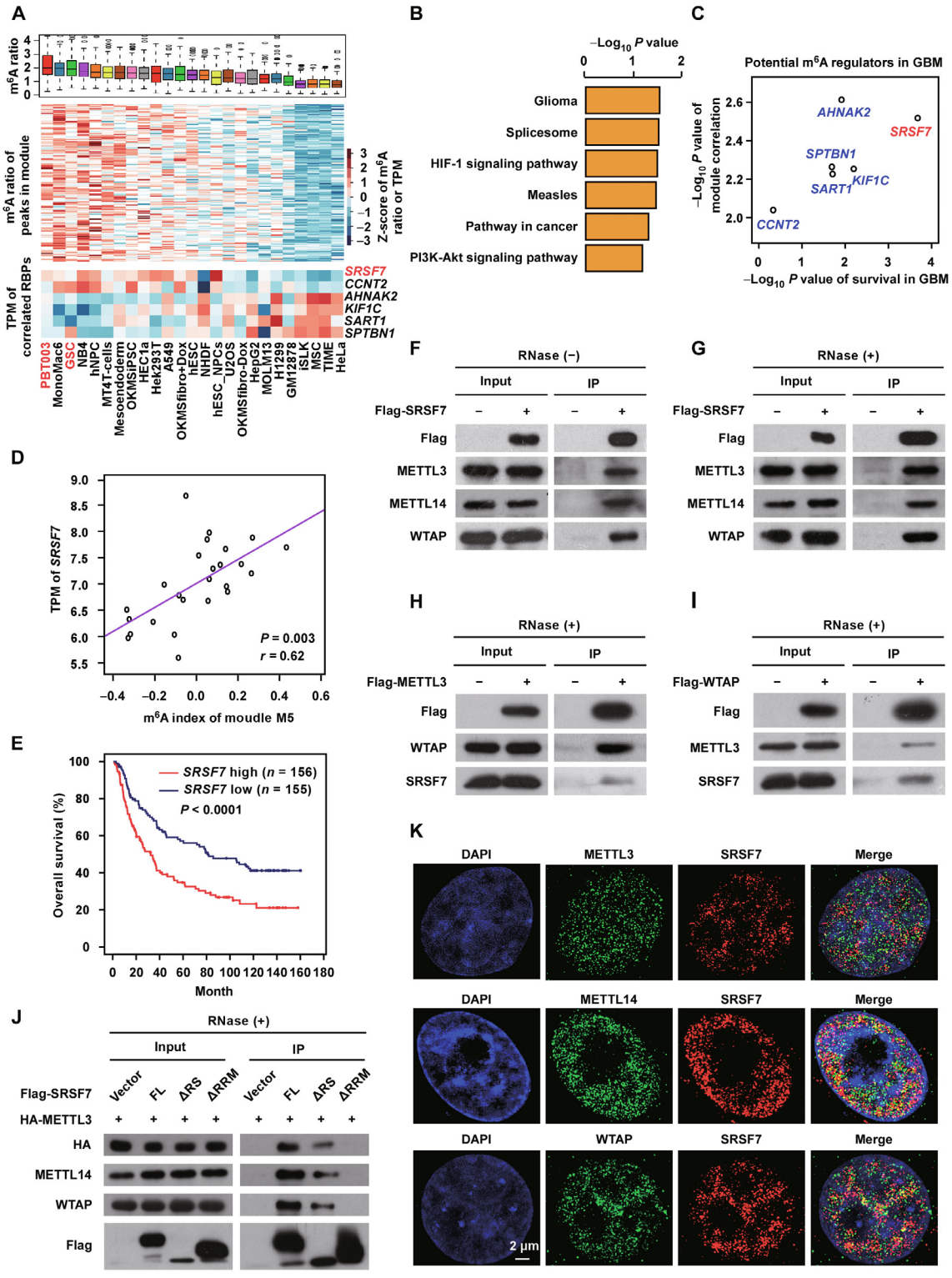
A
m6A ratio
m6A ratio of peaks in module
Z-score of m6A ratio or TPM
TPM of correlated RBPs
SRSF7
CCNT2
AHNAK2
KIF1C
SART1
SPTBN1
PBT003
MonoMac6
GSC
NB4
hNPC
MT41-cells
Mesoendoderm
OKMSiPSC
HEC1a
Hek293T
A549
OKMSfibro+Dox
hESC
NHDF
hESC_NPCs
U2OS
OKMSfibro-Dox
HepG2
MOLM13
H1299
GM12878
iSLK
MSC
TIME
HeLa
B
−Log10 P value
Glioma
Splicesome
HIF-1 signaling pathway
Measles
Pathway in cancer
PI3K-Akt signaling pathway
C
Potential m6A regulators in GBM
−Log10 P value of module correlation
−Log10 P value of survival in GBM
AHNAK2
SRSF7
SPTBN1
KIF1C
SART1
CCNT2
D
TPM of SRSF7
m6A index of moudle M5
P = 0.003
r = 0.62
E
SRSF7 high (n = 156)
SRSF7 low (n = 155)
P < 0.0001
Overall survival (%)
Month
F
RNase (−)
Input
IP
Flag-SRSF7
Flag
METTL3
METTL14
WTAP
G
RNase (+)
H
Flag-METTL3
SRSF7
I
Flag-WTAP
J
Vector
FL
ΔRS
ΔRRM
HA-METTL3
HA
K
DAPI
METTL3
METTL14
WTAP
SRSF7
Merge
2 μm

protein-coding regions, which was distinct from m^{6}A peaks; while the peaks colocalized with m^{6}A peaks were enriched at both 5′ end and 3′ end (Figure 2C, Figure S2H), further suggesting that SRSF7 specifically regulates only a portion of m^{6}A peaks other than global regulation.

We were then interested in whether SRSF7 binding were related to the m^{6}A alteration due to *SRSF7* depletion. We found that although the overall m^{6}A ratios of all m^{6}A peaks do not change upon *SRSF7* knockdown, the m^{6}A ratios of m^{6}A peaks colocalized with SRSF7 iCLIP-seq peaks were significantly down-regulated upon *SRSF7* knockdown (Figure 2D), suggesting that SRSF7 can only promote m^{6}A modification near its binding sites. As compared with the m^{6}A peaks unbound by SRSF7, the m^{6}A ratio of SRSF7-bound m^{6}A peaks was significantly down-regulated due to *SRSF7* knockdown (Figure 2E), indicating that SRSF7 specifically facilitates the m^{6}A modification near its binding sites. As shown in Figure 2F, we also revealed significant enrichment of SRSF7 iCLIP-seq peaks in (or overlap with) the down-regulated m^{6}A peaks upon *SRSF7* knockdown. In addition, the SRSF7-binding sites were significantly enriched in m^{6}A peaks down-regulated upon *SRSF7* knockdown as compared with the up-regulated and unchanged m^{6}A peaks (Figure 2G), further supporting that SRSF7 binding results in locally enhanced other than decreased m^{6}A methylation. On the other hand, although the module was constructed from diverse cell lines, the SRSF7-binding sites in U87MG cells were still marginally significantly enriched ($P = 0.03$) in the orange module, which is a larger module merged by M5 and other 4 correlated modules, as compared with other modules. The m^{6}A peaks in the orange module were also significantly down-regulated upon *SRSF7* knockdown as compared with the m^{6}A peaks in other modules (Figure S2I), suggesting that SRSF7 promotes the m^{6}A modification of this module.

SRSF7 significantly regulates gene expression through regulating m^{6}A

We then studied whether SRSF7 affects the gene expression through regulating m^{6}A in U87MG cells. The expression levels of 1012 and 1275 genes were up-regulated and down-regulated, respectively, due to *SRSF7* knockdown (Figure S3A). GO enrichment analysis found that the down-regulated genes were enriched in terms such as cell division, cell migration, and cell cycle (Figure S3B), consistent with the GO terms enriched in differentially methylated genes (Figure S2E). However, the up-regulated genes were enriched in terms macroautophagy, vesicle docking, and protein transport (Figure S3C), which were quite different from the GO terms enriched in differentially methylated genes (Figure S2E). Gene set enrichment analysis (GSEA) also supported that the gene expression changes were involved in cell division, cell cytoskeleton, and cell cycle (Figure S3D–F). We found that both the up-regulated genes and down-regulated genes were significantly enriched for m^{6}A modified genes as compared with the genes without expression change ($P = 4.8 \times 10^{-14}$ for up-regulated genes; $P = 3.2 \times 10^{-20}$ for down-regulated genes; two-tailed Chi-square test; Figure 2H). This result suggests that SRSF7 can both up-regulate and down-regulate gene expression through m^{6}A, consistent with the previous reports that m^{6}A has dual effects on gene expression depends on how these m^{6}A sites are recognized by diverse m^{6}A readers [27,31–33]. To further clarify the direct effects of SRSF7, we investigated the effects of SRSF7 binding on gene expression though regulating m^{6}A. As shown in Figure 2I, the genes with SRSF7-targeted m^{6}A peaks were overall significantly down-regulated as compared with unmethylated genes upon *SRSF7* knockdown ($P = 3.6 \times 10^{-11}$, two-tailed Wilcoxon test; Figure 2I).

Artificially tethering SRSF7 on RNA directs *de novo* m^{6}A methylation through recruiting METTL3

We then performed a tethering assay to test whether direct tethering of SRSF7 protein was sufficient to dictate the m^{6}A modification nearby in U87MG cells. For this purpose, we respectively fused the full-length coding sequences (CDSs) of SRSF7 and METTL3 with λ peptide, which can specifically recognizes BoxB RNA [44]. We utilized a previously established F-luc-5BoxB luciferase reporter, which has five BoxB sequence in the 3′ UTR and a m^{6}A motif (GGACU) 73 bp

Figure 1 SRSF7 is a potential m^{6}A regulator that interacts with m^{6}A methyltransferase complex

A. The Box plot (upper panel) and heatmap (middle panel) representing the m^{6}A ratios of the m^{6}A peaks within the co-methylation module M5 as well as the heatmap (lower panel) representing the gene expression patterns of the RBPs that significantly correlated with the m^{6}A indexes of M5. The cell lines were sorted according to the m^{6}A indexes of M5, and GBM cell lines were colored red. **B.** GO enrichment analysis of corresponding genes in module M5. **C.** The Y-axis represents the log-transformed *P* values of the correlations between the gene expression of 6 RBPs and the m^{6}A indexes of co-methylation module M5; the X-axis represents the log-transformed *P* values of the overall survival of these 6 RBPs in GBM patients. **D.** Scatter plot representing the correlations between the expression of *SRSF7* and m^{6}A indexes of module M5 across 25 cell lines. The *P* value and correlation coefficient are indicated at the bottom right corner. **E.** Kaplan–Meier analysis of overall survival based on *SRSF7* expression of GBM patients from CGGA dataset. **F.** and **G.** Western blots showing the interactions of Flag-tagged SRSF7 with endogenous METTL3, METTL14, and WTAP without (F) and with (G) RNase treatment in U87MG cells. **H.** and **I.** Western blots showing the interactions of Flag-tagged METTL3 (H) and WTAP (I) with endogenous SRSF7 with RNase treatment in U87MG cells. **J.** Western blot showing the interactions of Flag-tagged FL and truncated SRSF7 with HA-tagged METTL3, endogenous METTL14, and endogenous WTAP with RNase treatment in U87MG cells. **K.** 3D-SIM imaging indicating the colocalization of SRSF7 with METTL3, METTL14, and WTAP in the nucleus. Scale bar, 2 μm. M5, module 5; RBP, RNA-binding protein; GBM, glioblastoma; TPM, transcripts per million; GO, Gene Ontology; CGGA, Chinese Glioma Genome Atlas; IP, immunoprecipitation; FL, full-length; ΔRS, truncated SRSF7 with arginine/serine domain deleted; ΔRRM, truncated SRSF7 with RNA recognition motif domain deleted; HA, hemagglutinin; 3D-SIM, 3D structured illumination microscopy; DAPI, 4′,6-diamidino-2-phenylindole.

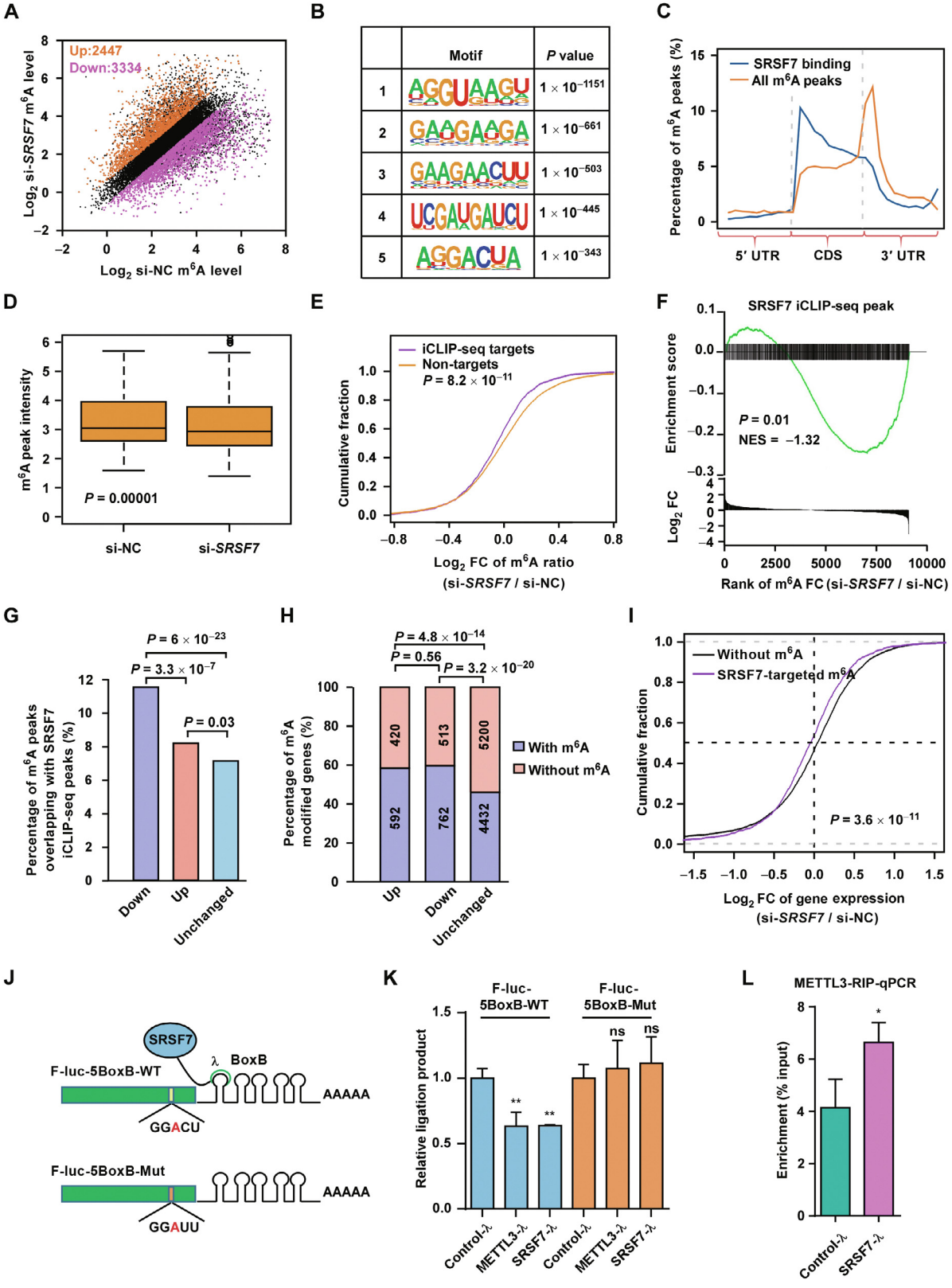
A
Up:2447
Down:3334
Log2 si-SRSF7 m6A level
Log2 si-NC m6A level
B
Motif
P value
1 × 10−1151
1 × 10−661
1 × 10−503
1 × 10−445
1 × 10−343
C
SRSF7 binding
All m6A peaks
Percentage of m6A peaks (%)
5′ UTR
CDS
3′ UTR
D
m6A peak intensity
P = 0.00001
si-NC
si-SRSF7
E
iCLIP-seq targets
Non-targets
P = 8.2 × 10−11
Cumulative fraction
Log2 FC of m6A ratio
(si-SRSF7 / si-NC)
F
SRSF7 iCLIP-seq peak
Enrichment score
P = 0.01
NES = −1.32
Log2 FC
Rank of m6A FC (si-SRSF7 / si-NC)
G
P = 6 × 10−23
P = 3.3 × 10−7
P = 0.03
Percentage of m6A peaks overlapping with SRSF7 iCLIP-seq peaks (%)
Down
Up
Unchanged
H
P = 4.8 × 10−14
P = 0.56
P = 3.2 × 10−20
Percentage of m6A modified genes (%)
420
513
5200
592
762
4432
With m6A
Without m6A
Up
Down
Unchanged
I
Without m6A
SRSF7-targeted m6A
P = 3.6 × 10−11
Cumulative fraction
Log2 FC of gene expression
(si-SRSF7 / si-NC)
J
SRSF7
λ BoxB
F-luc-5BoxB-WT
AAAAA
GGACU
F-luc-5BoxB-Mut
AAAAA
GGAUU
K
F-luc-5BoxB-WT
F-luc-5BoxB-Mut
ns
ns
Relative ligation product
Control-λ
METTL3-λ
SRSF7-λ
Control-λ
METTL3-λ
SRSF7-λ
L
METTL3-RIP-qPCR
Enrichment (% input)
Control-λ
SRSF7-λ

upstream of the stop codon (Figure 2J) [34]. We found that tethering SRSF7 and METTL3 could both significantly up-regulate the modification of m^{6}A site on the reporter to the similar degree using single-base elongation- and ligation-based quantitative polymerase chain reaction (qPCR) amplification (SELECT) method [45] (Figure 2K), indicating that SRSF7 can similarly dictate the methylation of nearby m^{6}A site as METTL3. A disruptive synonymous point mutation in the m^{6}A motif, which changes the GGACU to GGAUU, completely disrupted the effects on m^{6}A change by tethering SRSF7 and METTL3, respectively (Figure 2K), indicating the high reliability of the tethering assay. In addition, we found that binding of METTL3 on F-luc mRNA was significantly up-regulated when tethering SRSF7 to F-luc-5BoxB, indicating that SRSF7 promotes the installation of m^{6}A through recruiting METTL3 (Figure 2L).

SRSF7 specifically targets and facilitates the methylation of m^{6}A sites on genes involved in cell proliferation and migration

Since SRSF7 iCLIP-seq peaks are significantly enriched in down-regulated m^{6}A peaks upon *SRSF7* knockdown (Figure 2G), to further dissect the specific m^{6}A targets that directly regulated by SRSF7 binding, we intersected the 40,476 SRSF7 iCLIP-seq peaks and 3334 down-regulated m^{6}A peaks upon *SRSF7* knockdown, and obtained 911 SRSF7 directly regulated m^{6}A peaks in 760 genes (**Figure 3**A; Table S2). As shown in Figure 3B, the distribution of SRSF7 directly regulated m^{6}A peaks was still similar as the canonical distribution of m^{6}A peaks, suggesting that SRSF7 are not accounting for the formation of the canonical topology of m^{6}A like VIRMA [34]. GO and KEGG enrichment analyses revealed that the genes with SRSF7 directly regulated m^{6}A peaks were mainly involved in cell migration, cell adhesion, cell proliferation, glioma, cell cycle, and pathways in cancer (Figure 3C, Figure S4A). In contrast, the genes with SRSF7 iCLIP-seq peaks not colocalized with m^{6}A peaks were enriched in totally different terms which were not directly related to cell proliferation and migration (Figure S4B). The results suggest that the elevated expression of SRSF7 in GBM patients may involve in migration and proliferation of the cancer cells through regulating the m^{6}A methylation of corresponding genes.

To further validate the 911 SRSF7 directly regulated m^{6}A peaks, we then selected 3 m^{6}A peaks in 3 tumorigenic genes involved in migration or proliferation of GBM, respectively. All of the 3 peaks in PDZ-binding kinase (*PBK*), minichromosome maintenance complex component 4 (*MCM4*), and roundabout guidance receptor 1 (*ROBO1*) were successfully validated (Figure 3D and E, Figure S4C). We detected 4 single-nucleotide m^{6}A sites in the 3 m^{6}A peaks according to the public available miCLIP-seq data [46,47]. The methylation levels of the 4 m^{6}A sites in the 3 m^{6}A peaks (*PBK* at 1041 and 1071, *MCM4* at 1515, and *ROBO1* at 672) were significantly decreased upon *SRSF7* knockdown and *METTL3* knockdown, respectively, based on SELECT method [45] (Figure 3F–I), indicating that SRSF7 has similar effects of promoting m^{6}A modification as METTL3 on these selected m^{6}A sites. We also found that the binding efficiencies of METTL3, METTL14, and WTAP on the RNAs of these 3 genes were significantly reduced upon *SRSF7* knockdown based on RNA immunoprecipitation-quantitative polymerase chain reaction (RIP-qPCR) (Figure 3J–L). Collectively, these

Figure 2 SRSF7 specifically facilitates m^{6}A methylation near its binding sites via recruiting METTL3
A. Scatter plot showing the up-regulated (orange) and down-regulated (purple) m^{6}A peaks in si-*SRSF7* as compared with si-NC in U87MG cells. The numbers of the up-regulated and down-regulated peaks are indicated. **B.** The most significantly enriched motifs in the iCLIP-seq identified SRSF7-binding peaks. **C.** Normalized distributions of m^{6}A peaks and SRSF7 iCLIP-seq peaks across 5′ UTR, CDS, and 3′ UTR of mRNA. **D.** Box plot comparing the m^{6}A ratios of the SRSF7-targeted m^{6}A peaks in control and *SRSF7*-knockdown U87MG cells. **E.** Plot of cumulative fraction of $\log_2$ FC of m^{6}A ratios upon *SRSF7* knockdown using si-*SRSF7* for the m^{6}A peaks overlapping or non-overlapping with SRSF7 iCLIP-seq peaks. *P* value is determined by two-tailed Wilcoxon test. **F.** Plot of GSEA analysis displaying the distribution of SRSF7 iCLIP-seq peaks (upper panel) across the m^{6}A peaks ranked by $\log_2$ FC of m^{6}A ratios upon *SRSF7* knockdown (si-*SRSF7*) (lower panel). The m^{6}A peaks overlapping with SRSF7 iCLIP-seq peaks are indicated by vertical lines in the upper panel. The *P* value and NES of GSEA are indicated. **G.** Bar plot comparing the percentages of m^{6}A peaks overlapping with SRSF7 iCLIP-seq peaks for down-regulated, up-regulated, and unchanged m^{6}A peaks upon *SRSF7* knockdown, respectively. The pairwise *P* values of two-tailed Chi-square tests are indicated at the top. **H.** Bar plot comparing the percentages of m^{6}A modified genes for genes with down-regulated, up-regulated, and unchanged gene expression upon *SRSF7* knockdown, respectively. The pairwise *P* values of two-tailed Chi-square tests are indicated at the top. **I.** Plot of cumulative fraction of $\log_2$ FC of gene expression upon *SRSF7* knockdown for unmethylated genes and genes with SRSF7-targeted m^{6}A peaks, respectively. *P* value of two-tailed Wilcoxon test is indicated. **J.** Schematic diagram displaying the constructs of the SRSF7 tethering assay with GGACU m^{6}A motif (upper) and disruptive GGAUU motif (lower). **K.** Bar plot comparing the SELECT method measured relative ligation products, which anti-correlated with the m^{6}A levels, for the m^{6}A sites in F-luc-5BoxB without or with mutation in the m^{6}A motif in U87MG cells transfected with control-λ, SRSF7-λ, and METTL3-λ, respectively. Data are presented as mean ± SEM (n = 3). **, $P < 0.01$; ns, no significant difference. One-way ANOVA with Dunnett's post hoc test. **L.** Bar plot comparing the METTL3 RIP-qPCR enrichment of the F-luc mRNA in U87MG cells transfected with SRSF7-λ and control-λ, respectively. Data are presented as mean ± SEM (n = 3). *, $P < 0.05$. Student's two-tailed *t*-test. NC, negative control; iCLIP-seq, individual-nucleotide resolution UV crosslinking and immunoprecipitation combined with high throughput sequencing; UTR, untranslated region; CDS, coding sequence; FC, fold change; GSEA, gene set enrichment analysis; NES, normalized enrichment score; SELECT, single-base elongation- and ligation-based quantitative polymerase chain reaction amplification; SEM, standard error of mean; ANOVA, analysis of variance; RIP-qPCR, RNA immunoprecipitation-quantitative polymerase chain reaction.

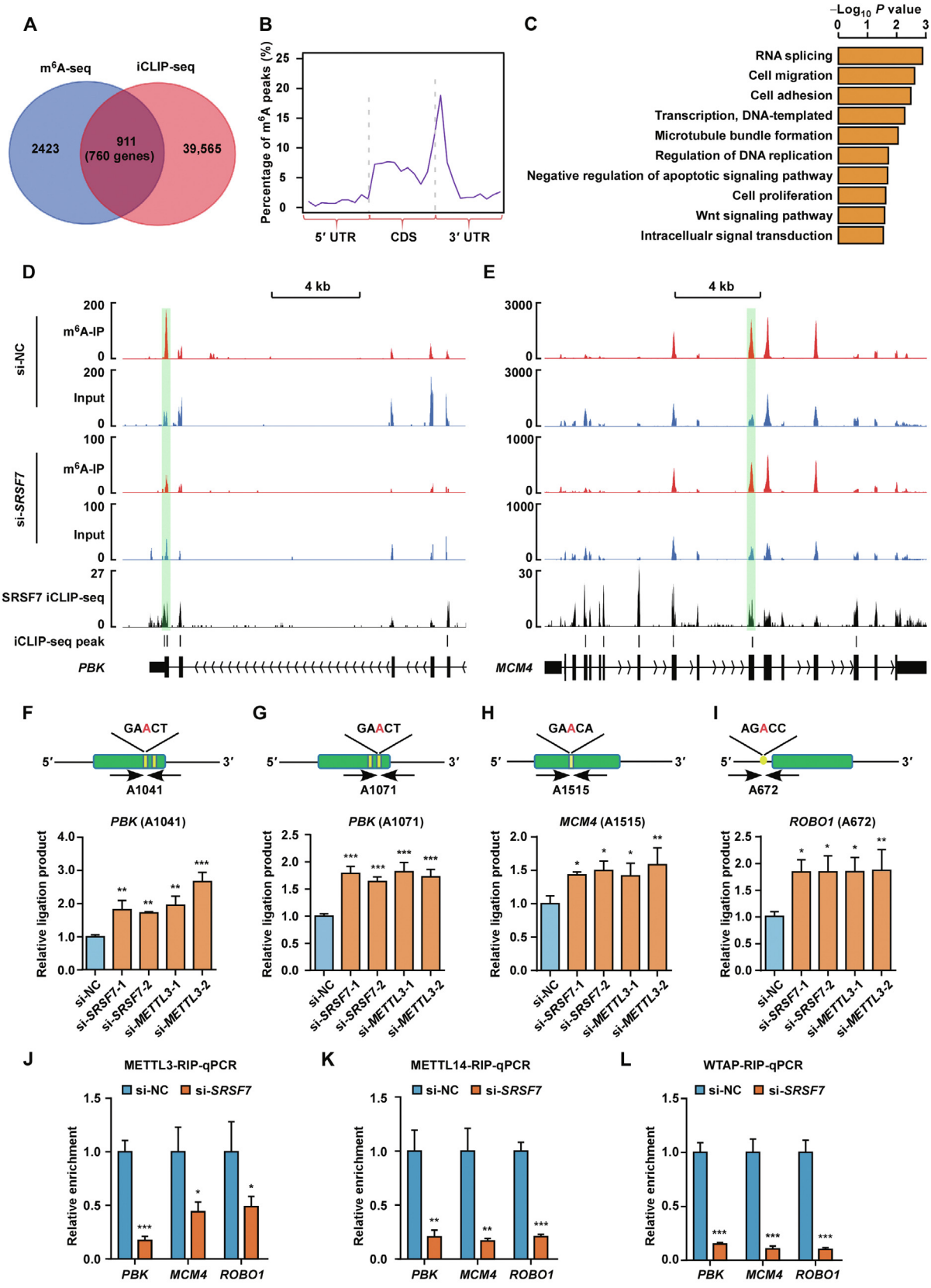
A
m6A-seq
iCLIP-seq
2423
911
(760 genes)
39,565
B
Percentage of m6A peaks (%)
5′ UTR
CDS
3′ UTR
C
−Log10 P value
RNA splicing
Cell migration
Cell adhesion
Transcription, DNA-templated
Microtubule bundle formation
Regulation of DNA replication
Negative regulation of apoptotic signaling pathway
Cell proliferation
Wnt signaling pathway
Intracellualr signal transduction
D
4 kb
si-NC
m6A-IP
Input
si-SRSF7
SRSF7 iCLIP-seq
iCLIP-seq peak
PBK
E
4 kb
MCM4
F
GAACT
A1041
PBK (A1041)
G
GAACT
A1071
PBK (A1071)
H
GAACA
A1515
MCM4 (A1515)
I
AGACC
A672
ROBO1 (A672)
Relative ligation product
si-NC
si-SRSF7-1
si-SRSF7-2
si-METTL3-1
si-METTL3-2
J
METTL3-RIP-qPCR
K
METTL14-RIP-qPCR
L
WTAP-RIP-qPCR
Relative enrichment
PBK
MCM4
ROBO1

results show that SRSF7 promotes m^{6}A modification on tumorigenic genes through recruiting METTL3.

SRSF7 promotes proliferation and migration of GBM cells partially dependent on METTL3

Since SRSF7 specifically regulates the m^{6}A modification of tumorigenic genes in GBM cells, we therefore wanted to confirm whether it plays important roles in GBM. We found that the expression of *SRSF7* was highly elevated in glioma specimens, especially in GBM (grade IV) tissues according to CGGA data (**Figure 4**A), which was confirmed by immunohistochemistry (IHC) in human glioma tissues (Figure 4B) and consistent with a previous report [10]. To further confirm this finding, we tested the mRNA expression of *SRSF7* in 11 GBM cell lines as well as normal human astrocytes (NHAs). We found that the mRNA expression of *SRSF7* was significantly elevated in most of the GBM cell lines, while the protein was highly expressed in all GBM cell lines as compared with NHAs (Figure 4C and D).

Because the genes with SRSF7 directly regulated m^{6}A peaks were enriched in cell proliferation- and migration-related GO terms (Figure 3C), we separately overexpressed and knocked down *SRSF7* in U87MG cells and LN229 cells, and then performed EdU staining, colony formation, and transwell assays to test the effects of SRSF7 on cell proliferation and migration. We found that overexpression of *SRSF7* prompted the cell proliferation and migration of these two cell lines (Figure 4E and F, Figure S5A). Consistently, depletion of *SRSF7* significantly impaired the proliferation and migration in U87MG and LN229 cell lines (Figure 4G and H, Figure S5B–D), and overexpression of *SRSF7* can rescue the inhibition of proliferation and migration caused by *SRSF7* knockdown (Figure S5E–G), which are similar as the effects of *METTL3* knockdown in the same cell lines [48,49]. Although METTL3 has been reported to regulate the stemness of GBM cells [48–51], the genes with SRSF7 directly regulated m^{6}A peaks have no enrichment of stemness-related terms (Figure 3C). Here, we found that neither knockdown or overexpression of *SRSF7* could affect the neurosphere formation in U87MG cells (Figure S5H), which suggesting that SRSF7 plays more specific roles in GBM than METTL3 through specific regulation of m^{6}A. To investigate the oncogenic role of SRSF7 in GBM cells *in vivo*, we utilized an intracranial xenograft tumor model, in which we transplanted *SRSF7*-knockdown as well as control U87MG stable cell lines into the nude mice. Consistent with the *in vitro* findings, *SRSF7* knockdown significantly inhibited the growth of glioma xenografts (Figure 4I–K). We further confirmed that SRSF7 cannot regulate the gene or protein expression of the core methyltransferase complex (**Figure 5**A, Figure S6A–E), and METTL3 or WTAP cannot regulate the expression of SRSF7 either in U87MG or LN229 cells (Figure S6F and G). In addition, *SRSF7* knockdown did not change the nuclear speckle localization of METTL3, METTL14, or WTAP (Figure S6H–J). The afromentioned results indicate that SRSF7 promotes the proliferation and migration, which are usually related to oncogenic roles, of GBM cells.

It has been reported that METTL3 plays oncogenic roles in GBM [52–55], we were therefore interested in whether SRSF7 plays oncogenic roles through specifically guiding METTL3 to oncogenic genes. We found that *METTL3* knockdown largely, although not completely, disrupted the effects of *SRSF7* overexpression on promoting the migration (Figure 5A–C) and proliferation (Figure 5D–F) of U87MG and LN229 cells, indicating that SRSF7 regulates migration and proliferation partially dependent on METTL3. The aforementioned results are consistent with our model that SRSF7 specifically guides METTL3 to the specific oncogenes and METTL3 takes in charge to install the m^{6}A on these RNAs.

SRSF7 promotes the proliferation and migration of GBM cells partially through the m^{6}A on *PBK* mRNA

We were then interested in the downstream targets of SRSF7 that mediated the proliferation and migration changes of GBM cells via m^{6}A. Out of the 760 genes with SRSF7 directly regulated m^{6}A peaks, *PBK* is the most significantly down-regulated gene upon *SRSF7* knockdown. Meanwhile, as shown in Figure 3D, F, and G, we have confirmed that *SRSF7* knockdown significantly reduced the m^{6}A levels of two m^{6}A sites on *PBK* (A1041 and A1071). PBK is also a serine/threonine protein kinase which is aberrantly overexpressed in various cancers and plays important roles in promoting the proliferation and migration of multiple cancers including glioma [56–60]. Based on the CGGA dataset, *PBK* is significantly highly expressed in WHO IV of glioma patients as compared with WHO II and WHO III, and the highly expression

Figure 3 SRSF7 specifically targets and facilitates the methylation of m^{6}A sites on genes involved in cell proliferation and migration
A. Venn diagram showing the overlapping of down-regulated m^{6}A peaks upon *SRSF7* knockdown and SRSF7 iCLIP-seq peaks. **B.** Normalized distribution of the overlapping m^{6}A peaks in (A) across 5′ UTR, CDS, and 3′ UTR of mRNA. **C.** GO enrichment of the corresponding genes with the overlapping m^{6}A peaks in (A). **D.** and **E.** Tracks displaying the read coverage of IPs and inputs of m^{6}A-seq as well as the SRSF7 iCLIP-seq on *PBK* and *MCM4*. The SRSF7 directly regulated m^{6}A peaks are highlighted in green. The Y-axes of si-NC and si-*SRSF7* were differently used to intuitionally indicate the m^{6}A differences other than expression differences. **F.–I.** Validation of m^{6}A changes of single-nucleotide m^{6}A sites on *PBK* at 1041 and 1071 (F and G), *MCM4* at 1515 (H), and *ROBO1* at 672 (I) using the SELECT method in U87MG cells transfected with scramble (si-NC), two siRNAs of *SRSF7* (si-*SRSF7*-1, si-*SRSF*-2), and two siRNAs of *METTL3* (si-*METTL3*-1, si-*METTL3*-2), respectively. The tested m^{6}A motifs are indicated on the schematic structures of mRNAs at the top panels. The green boxes represent protein-coding regions, the thin lines flanking the green boxes represent UTRs. Arrows indicate the primers for SELECT. Data are presented as mean ± SEM (n = 3). *, $P < 0.05$; **, $P < 0.01$; ***, $P < 0.001$. One-way ANOVA with Dunnett's post hoc test. **J.–L.** Bar plots comparing the RIP-qPCR determined relative enrichment of METTL3 (J), METTL14 (K), and WTAP (L) binding to the mRNAs of *PBK*, *MCM4*, and *ROBO1* in control and *SRSF7*-knockdown U87MG cells. Data are presented as mean ± SEM (n = 3). *, $P < 0.05$; **, $P < 0.01$; ***, $P < 0.001$. Student's two-tailed t-test.

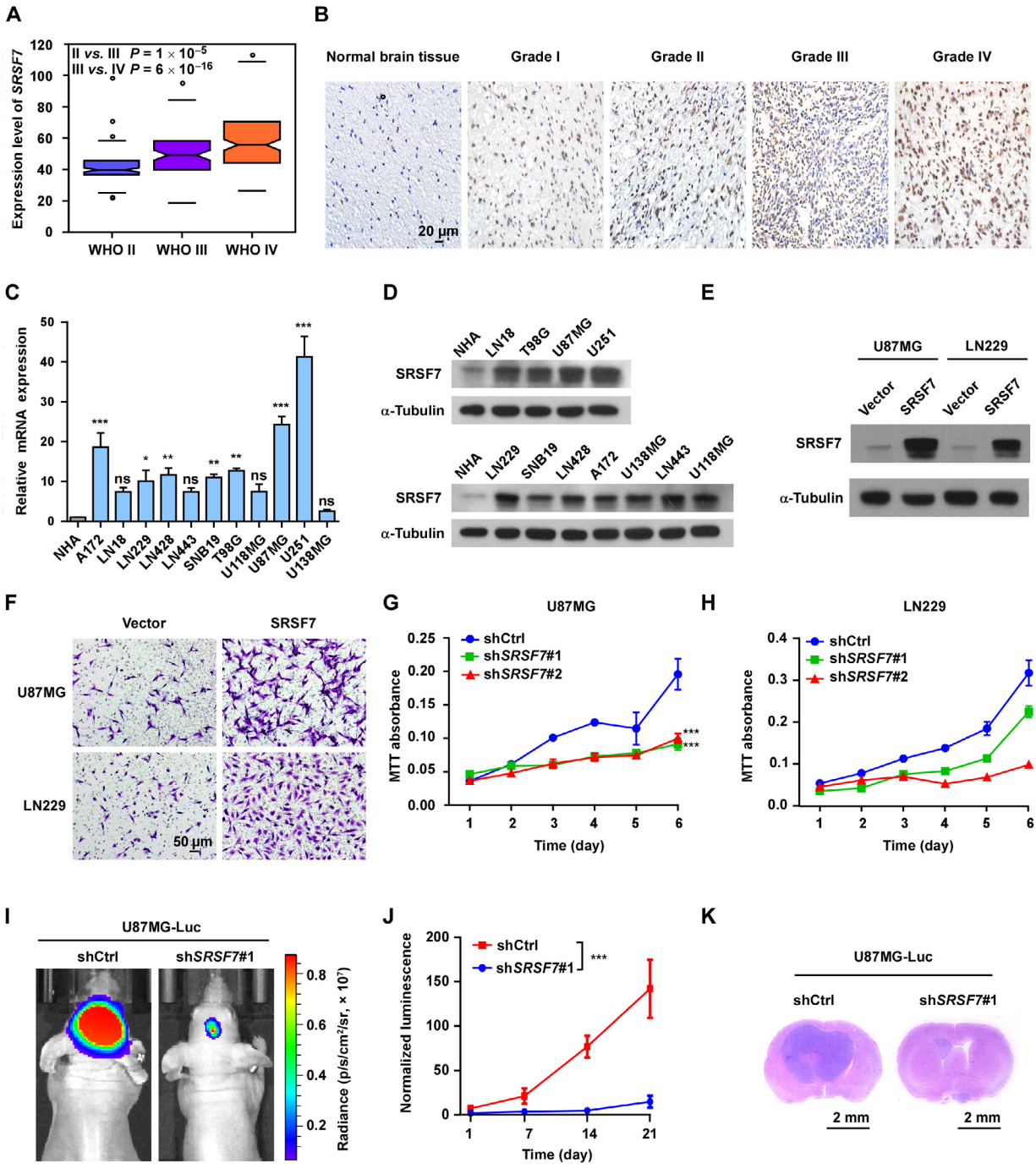
A
Expression level of SRSF7
II vs. III P = 1 × 10−5
III vs. IV P = 6 × 10−16
WHO II
WHO III
WHO IV
B
Normal brain tissue
Grade I
Grade II
Grade III
Grade IV
20 μm
C
Relative mRNA expression
NHA
A172
LN18
LN229
LN428
LN443
SNB19
T98G
U118MG
U87MG
U251
U138MG
D
SRSF7
α-Tubulin
E
U87MG
LN229
Vector
SRSF7
F
Vector
SRSF7
U87MG
LN229
50 μm
G
U87MG
shCtrl
shSRSF7#1
shSRSF7#2
MTT absorbance
Time (day)
H
LN229
I
U87MG-Luc
shCtrl
shSRSF7#1
Radiance (p/s/cm²/sr, × 10⁷)
J
Normalized luminescence
Time (day)
K
U87MG-Luc
shCtrl
shSRSF7#1
2 mm

of *PBK* is significantly associated with poor prognosis in GBM (Figure S7A and B). Furthermore, the gene expression of *PBK* is positively correlated with *SRSF7* and *METTL3* based on CGGA dataset (**Figure 6**A, Figure S7C), suggesting a regulatory role between them. We found that overexpression of *PBK* could partially rescue the *SRSF7*-knockdown induced inhibition of proliferation and migration of U87MG and LN229 cells (Figure 6B and C, Figure S7D and E), indicating that PBK is an important downstream target of SRSF7 and partially mediates the effects of SRSF7 on promoting the proliferation and migration of GBM cells. We were therefore interested in whether and how the expression of *PBK* was regulated by SRSF7.

First, we tested whether SRSF7 played a regulator role on *PBK* through regulating its m^{6}A. We found that *SRSF7* knockdown significantly decreased the mRNA and protein expression of *PBK* in U87MG cells (Figure 6D and E). Overexpression of *SRSF7* significantly up-regulated the gene expression of *PBK*, and *METTL3* knockdown largely disrupted the effect of *SRSF7* overexpression on the expression of *PBK* in U87MG cells (Figure 6F, Figure S7F and G), indicating that SRSF7 regulates *PBK* depends on METTL3.

We then asked how the m^{6}A of *PBK* affects its expression. We found that *SRSF7* knockdown also significantly promoted the degradation of *PBK* mRNA (Figure 6G), suggesting that SRSF7 increases *PBK* gene expression through promoting the stability of *PBK* mRNA. To further confirm that this regulation of mRNA stability depends on the m^{6}A of *PBK*, we introduced two synonymous A-to-G mutations to disrupt the two m^{6}A sites on *PBK* (Figure 6H). We found that the overexpressed mutant *PBK* exhibited significantly lower expression and lower stability of *PBK* mRNA than the overexpressed wild-type *PBK* (Figure 6I and J), suggesting that the modification of the two m^{6}A sites on *PBK* is essential for the stability of *PBK* mRNA. Because m^{6}A readers IGF2BP1–3 have been reported to promote the stabilities of mRNAs and play oncogenic roles in multiple cancers [31]. We then tested whether *IGF2BP2*, a gene significantly up-regulated in GBM, could affect the mRNA stability of *PBK* through binding the m^{6}A sites. We found that knockdown of *IGF2BP2* decreased the expression and stability of endogenous *PBK* mRNA (Figure 6K, Figure S7H), which is consistent with the finding that the gene expression of *IGF2BP2* is positively correlated with *PBK* based on CGGA dataset (Figure S7I). Knockdown of *IGF2BP2* could also significantly decrease the stability of the exogenously overexpressed wild-type *PBK* other than mutant *PBK* with the two m^{6}A sites disrupted (Figure 6L), suggesting that the regulatory role of IGF2BP2 on the stability of *PBK* depends on the two m^{6}A sites.

SRSF7 regulates m^{6}A independent of alternative splicing and APA

Since SRSF7 was previously recognized as a splicing factor [2–4], to test whether SRSF7 can regulate alternative splicing in U87MG cells, we analyzed the differential alternative splicing of input RNAs between *SRSF7*-knockdown and control using rMATS [61]. We found 1344 differentially spliced events, including 734 skipped exons (SEs), 222 retained introns (RIs), 129 alternative spliced 5′ splice sites (A5SSs), 173 alternative spliced 3′ splice sites (A3SSs), and 86 mutually exclusive exons (MXEs). Of note, none of *PBK*, *MCM4*, or *ROBO1* has alternative splicing change upon *SRSF7* knockdown. We then used rMAPS2 [62] to study the enrichment of SRSF7 iCLIP-seq peaks near the splice sites of differentially spliced SE events, which are the most abundant type for reliable analyses. We found that the iCLIP-seq targets of SRSF7 were significantly enriched in the alternative exons of the differentially spliced evens, suggesting that SRSF7 binding directs the splicing changes (**Figure 7**A). GO analysis revealed that the genes with significant splicing changes were also enriched in functional terms "cell-cell adhesion" and "cell cycle" (Figure 7B), suggesting that SRSF7 can also regulate cell proliferation and migration through alternative splicing. For the 760 genes with SRSF7 directly regulated m^{6}A peaks, only 102 (13.4%) of them had significant splicing changes upon *SRSF7* knockdown (Figure 7C), which represented a non-significant overlap that could easily occur by random chance ($P = 0.3$, two-tailed Chi-square test). For the 129 m^{6}A peaks in the 102 genes, only 36 peaks in 28 genes were localized within the local regions of differentially splicing events spanning between upstream exons to downstream exons, of which only 7 m^{6}A peaks were located

Figure 4 SRSF7 promotes proliferation and migration of GBM cells

A. Box plot comparing the expression of *SRSF7* during GBM patients of different stages from CGGA dataset. *P* values of two-tailed Student's *t*-test are indicated. **B.** IHC staining of SRSF7 in normal brain and glioma specimens. Scale bar, 20 μm. **C.** Bar plot comparing the relative mRNA expression levels of *SRSF7* in 11 GBM cell lines as well as NHAs. Data are presented as mean ± SEM ($n = 2$). *, $P < 0.05$; **, $P < 0.01$; ***, $P < 0.001$; ns, no significant difference. One-way ANOVA with Dunnett's post hoc test. **D.** Western blot comparing the protein levels of SRSF7 in 11 GBM cell lines as well as NHAs. **E.** Western blot showing efficient overexpression of *SRSF7* in U87MG and LN229 cells. **F.** Representative images of transwell migration assay in U87MG and LN229 cells overexpressing *SRSF7*. Scar bar, 50 μm. **G.** and **H.** The cell viability of *SRSF7*-knockdown and control U87MG (G) and LN229 (H) cells measured by MTT assay at indicated time points. Data are presented as mean ± SEM ($n = 3$). ***, $P < 0.001$. Two-way ANOVA with Dunnett's post hoc test. **I.** Representative bioluminescence images of mice bearing the intracranial glioma xenograft formed by U87MG cells transduced with shCtrl and sh*SRSF7*, respectively. **J.** Line graph showing the normalized luminescence of intracranial glioma xenograft tumors formed by U87MG cells transduced with shCtrl and sh*SRSF7*, respectively. Data are presented as mean ± SEM ($n = 6$). ***, $P < 0.001$. Student's two-tailed *t*-test. **K.** Representative images of H&E staining of glioma tissue sections from indicated mice. Scale bar, 2 mm. IHC, immunohistochemistry; NHA, normal human astrocyte; WHO, world health organization; MTT, 3-(4,5-dimethylthiazole-2-yl)-2,5-diphenyl tetrazolium bromide; shCtrl, control shRNA; sh*SRSF7*, *SRSF7* shRNA; H&E staining, hematoxylin-eosin staining.

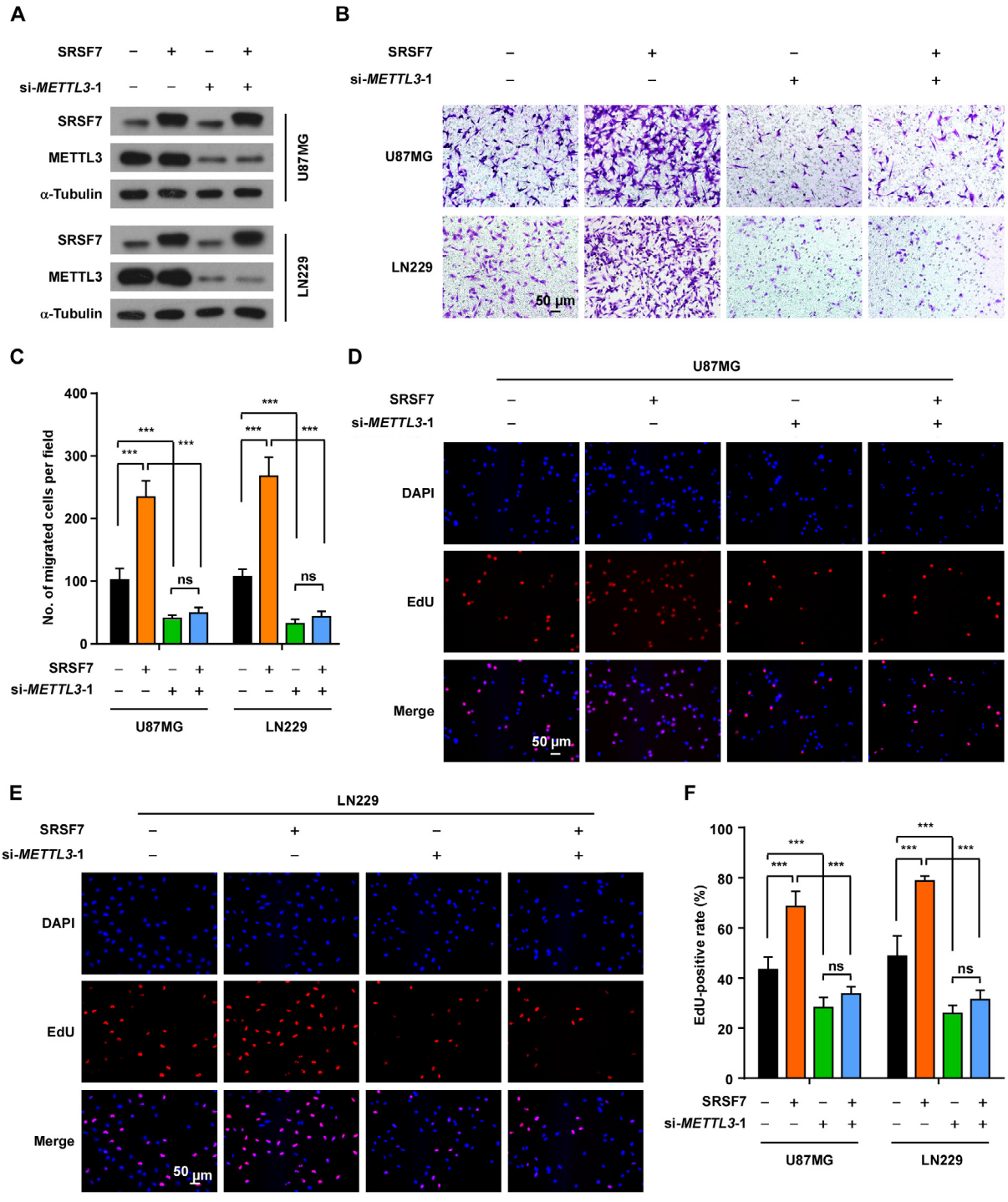

Figure 5 SRSF7 promotes the proliferation and migration of GBM cells partially dependent on METTL3

A. Western blot showing the protein levels of SRSF7 and METTL3 in *SRSF7*-overexpressed U87MG and LN229 cells transfected without or with si-*METTL3*-1 as indicated. **B.** and **C.** Representative images (B) and bar plot (C) comparing the number of migrated cells in transwell migration assay in *SRSF7*-overexpressed U87MG and LN229 cells transfected without or with si-*METTL3*-1 as indicated. Data are presented as mean ± SEM ($n = 5$). ***, $P < 0.001$; ns, no significant difference. One-way ANOVA with Tukey's post hoc test. Scar bars, 50 μm. **D.** and **E.** Representative images of EdU staining in *SRSF7*-overexpressed U87MG (D) and LN229 (E) cells transfected without or with si-*METTL3*-1 as indicated. Scar bar, 50 μm. **F.** Bar plot comparing the EdU positive rate of EdU staining in *SRSF7*-overexpressed U87MG and LN229 cells transfected without or with si-*METTL3*-1 as indicated. Data are presented as mean ± SEM ($n = 5$). *, $P < 0.05$; ***, $P < 0.001$; ns, no significant difference. One-way ANOVA with Tukey's post hoc test. EdU, 5-ethynyl-2′-deoxyuridine.

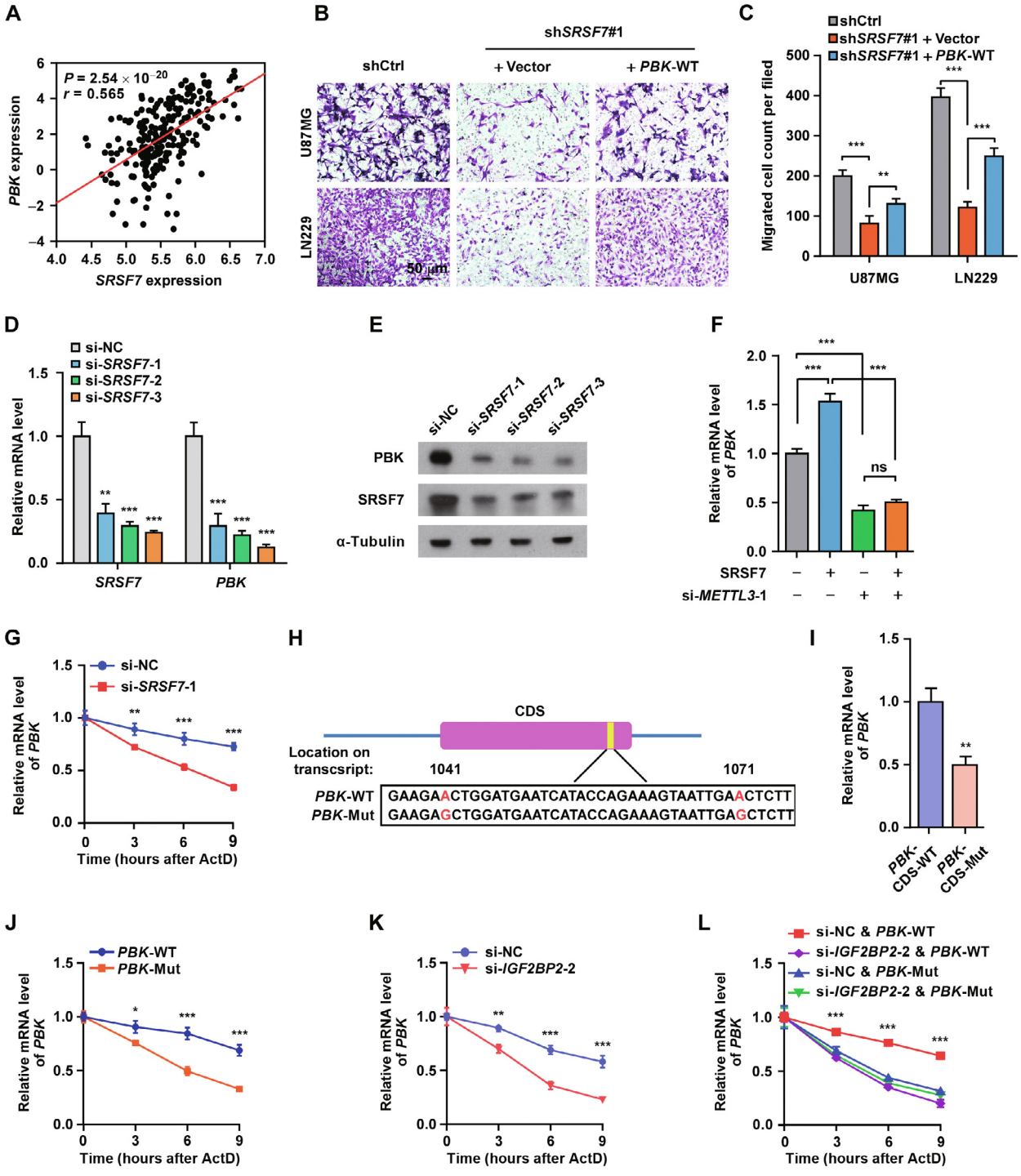
A
P = 2.54 × 10−20
r = 0.565
PBK expression
SRSF7 expression
B
shSRSF7#1
shCtrl
+ Vector
+ PBK-WT
U87MG
LN229
50 μm
C
shCtrl
shSRSF7#1 + Vector
shSRSF7#1 + PBK-WT
Migrated cell count per filed
U87MG
LN229
D
si-NC
si-SRSF7-1
si-SRSF7-2
si-SRSF7-3
Relative mRNA level
SRSF7
PBK
E
si-NC
si-SRSF7-1
si-SRSF7-2
si-SRSF7-3
PBK
SRSF7
α-Tubulin
F
Relative mRNA level of PBK
ns
SRSF7
si-METTL3-1
G
si-NC
si-SRSF7-1
Relative mRNA level of PBK
Time (hours after ActD)
H
CDS
Location on transcsript:
1041
1071
PBK-WT GAAGAACTGGATGAATCATACCAGAAAGTAATTGAACTCTT
PBK-Mut GAAGAGCTGGATGAATCATACCAGAAAGTAATTGAGCTCTT
I
Relative mRNA level of PBK
PBK-CDS-WT
PBK-CDS-Mut
J
PBK-WT
PBK-Mut
Relative mRNA level of PBK
Time (hours after ActD)
K
si-NC
si-IGF2BP2-2
Relative mRNA level of PBK
Time (hours after ActD)
L
si-NC & PBK-WT
si-IGF2BP2-2 & PBK-WT
si-NC & PBK-Mut
si-IGF2BP2-2 & PBK-Mut
Relative mRNA level of PBK
Time (hours after ActD)

within the alternative exons or regions. The aforementioned results indicate that SRSF7 regulates m^{6}A and alternative splicing independently through distinct binding sites, consistent with our observation that only a part of SRSF7 proteins colocalize with METTL3 and only a part of SRSF7-binding sites can regulate m^{6}A.

Since SRSF7 was also reported to regulate APA of RNAs [5], we also analyzed the differential APAs of input RNAs between *SRSF7*-knockdown and control U87MG cells using DaPars [63]. We found that only 14 APA events were significantly changed (Figure 7D), and none of the SRSF7 directly regulated m^{6}A peaks was located within the 14 APA regions regulated by SRSF7, suggesting noninterference between SRSF7 regulated m^{6}A and APA.

Discussion

m^{6}A has been reported to play important roles in diverse systems through different targets. There are widespread m^{6}A sites on most of the genes with diverse functions. It is very important for cells to dynamically coordinate the methylation of different genes to fulfil specific functions. In this study, we found that SRSF7 specifically regulates the m^{6}A on genes involved in cell proliferation and migration, which demonstrates an important role of RBP-mediated specific regulation of m^{6}A in co-regulating and coordinating a batch of related m^{6}A sites in order to modulate the specific functions in cells. These diverse specific m^{6}A regulators provide a versatile toolkit for cells to deal with various inner and outer stimulates. On the other hand, widespread involvement of RBPs in regulating m^{6}A suggests that the m^{6}A signaling pathways are deeply involved in the regulatory network of genes. Therefore, other signaling or regulatory pathways can modulate the m^{6}A through regulating the RBPs in order to fulfil the downstream functions. It is very possible that more and more important functional roles of RBP-mediated specific regulation of m^{6}A will be revealed in the future.

SRSF7 is an adaptor of NXF1, which exports mature RNAs out of nucleus, and plays important roles in coupling RNA alternative splicing and APA to mRNA export [5]. Here, we reveals a novel role for SRSF7 as a regulator of m^{6}A methylation via recruiting METTL3. It is very possible that SRSF7 may also couple m^{6}A methylation to mRNA export, and in this way the specific RNAs must be methylated before export. RBM15, a component of methyltransferase complex, is also an adaptor of NXF1 [64], furthering suggesting that methylation and export could be linked by a series of m^{6}A regulators with RNA-binding specificities.

Interaction of SRSF7 with the nucleic m^{6}A reader YTHDC1 has been reported by different groups [65,66]. Xiao et al. found that SRSF7 does not mediate the splicing change regulated by YTHDC1 [65]. While Kasowitz et al. proposed that YTHDC1 regulates APA through recruiting SRSF7 [66]. The interactions of SRSF7 with both writers and readers of m^{6}A suggest that SRSF7 may also work to coordinate the feedback between writing and reading of m^{6}A. On the other hand, although the association between m^{6}A and APA has been reported in multiple studies, the mechanism is not clear yet [34,66–68]. Our finding that SRSF7 specifically regulates m^{6}A may provide a novel potential mechanism that links m^{6}A and APA by SRSF7.

We found that *SRSF7* knockdown did not affect the overall peak intensities of all m^{6}A peaks, but the overall peak intensities of SRSF7-targeted m^{6}A peaks were significantly downregulated upon *SRSF7* knockdown. The indicated fact that SRSF7 only regulates a small portion of m^{6}A sites may be a

Figure 6 SRSF7 promotes the proliferation and migration of GBM cells partially through the m^{6}A on *PBK* mRNA

A. Scatter plot showing the correlation between *SRSF7* and *PBK* gene expression across GBM patients from CGGA dataset. The *P* value and correlation coefficient are indicated. **B.** and **C.** Representative images (B) and bar plot (C) comparing the number of migrated cells in transwell migration assay in U87MG and LN229 cells upon *SRSF7* knockdown and rescue by co-transducing FL WT *PBK* CDS region. Data are presented as mean ± SEM ($n = 5$). **, $P < 0.01$; ***, $P < 0.001$. One-way ANOVA with Tukey's post hoc test. Scar bar, 50 μm. **D.** Bar plot showing the relative mRNA levels of *SRSF7* and *PBK* in U87MG cells transfected with scramble (si-NC) and three different siRNAs of *SRSF7* (si-*SRSF7*-1–3), respectively. Data are presented as mean ± SEM ($n = 3$). **, $P < 0.01$; ***, $P < 0.001$. Student's two-tailed *t*-test. **E.** Western bolt comparing the protein levels of SRSF7 and PBK in U87MG cells transfected with scramble (si-NC) and three different siRNAs of *SRSF7* (si-*SRSF7*-1–3), respectively. **F.** Bar plot showing the relative mRNA levels of *PBK* in *SRSF7*-overexpressed U87MG cells transfected without or with si-*METTL3*-1 as indicated. Data are presented as mean ± SEM ($n = 3$). ***, $P < 0.001$; ns, no significant difference. One-way ANOVA with Tukey's post hoc test. **G.** Relative mRNA levels of *PBK* after ActD treatment at indicated time points in U87MG cells transfected with scramble (si-NC) and siRNA of *SRSF7* (si-*SRSF7*-1), respectively. Data are presented as mean ± SEM ($n = 3$). **, $P < 0.01$; ***, $P < 0.001$. Two-way ANOVA with Bonferroni's post hoc test. **H.** Schematic diagram showing the mutation of the two m^{6}A sites in the *PBK* CDS region. **I.** Relative mRNA levels of *PBK* in U87MG cells transfected with FL WT or Mut *PBK* CDS region for 48 h. Data are presented as mean ± SEM ($n = 3$). **, $P < 0.01$. Student's two-tailed *t*-test. **J.** Relative mRNA levels of *PBK* after ActD treatment at indicated time points in U87MG cells transfected with FL WT and Mut *PBK* CDS regions, respectively. Data are presented as mean ± SEM ($n = 3$). *, $P < 0.05$; ***, $P < 0.001$. Two-way ANOVA with Bonferroni's post hoc test. **K.** Relative mRNA levels of *PBK* after ActD treatment at indicated time points in U87MG cells transfected with scramble (si-NC) and siRNA of *IGF2BP2* (si-*IGF2BP2*-2), respectively. Data are presented as mean ± SEM ($n = 3$). **, $P < 0.01$; ***, $P < 0.001$. Two-way ANOVA with Bonferroni's post hoc test. **L.** Relative mRNA levels of *PBK* after ActD treatment at indicated time points in WT *PBK* or Mut *PBK* overexpressed U87MG cells transfected with scramble (si-NC) and siRNA of *IGF2BP2* (si-*IGF2BP2*-2), respectively. Data are presented as mean ± SEM ($n = 3$). ***, $P < 0.001$. Two-way ANOVA with Dunnett's post hoc test. ActD, actinomycin D; WT, wild-type; Mut, mutant.

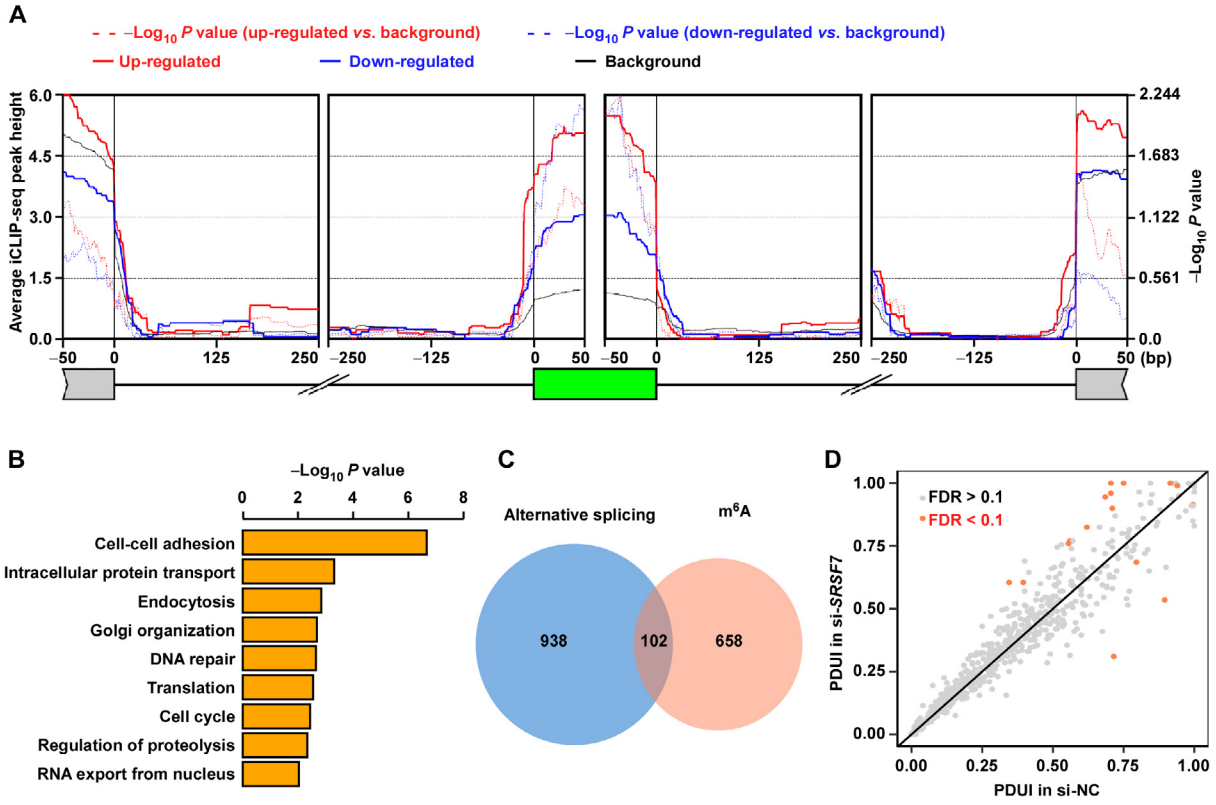

Figure 7 SRSF7 regulates m^{6}A independent of alternative splicing and APA

A. rMAPS2-generated metagene plot showing the enrichment of SRSF7 iCLIP-seq peaks at the regions around corresponding splice sites of the differentially spliced SE events upon *SRSF7* knockdown. The green box represents the SE. **B.** GO enrichment of differentially spliced genes (all types) upon *SRSF7* knockdown. **C.** Venn diagram showing the overlap between differentially spliced genes (all types) and genes with SRSF7 directly regulated m^{6}A peaks. **D.** Scatter plot comparing the PDUI between control and *SRSF7*-knockdown U87MG cells. APA, alternative polyadenylation; SE, skipped exon; PDUI, percentage of distal poly(A) site usage index.

general feature of all specific regulators of m^{6}A; it represents the advantage of using specific m^{6}A regulators for cells that require precise regulation of a small portion of m^{6}A targets. As we have previously proposed, the specific regulators of m^{6}A may work in a similar way as splicing factors [39,69], which usually do not affect the global splicing levels but a small portion of cell-specific splicing events [38]. On the other hand, although we have proved that only down-regulated m^{6}A peaks upon *SRSF7* knockdown are enriched for SRSF7-binding sites, we cannot rule out that there are also indirect effects of *SRSF7* knockdown that up-regulates m^{6}A, which may counteract the direct effects of SRSF7. We found significant ($P < 1 \times 10^{-4}$) enrichment of 8 motifs in the up-regulated m^{6}A peaks using all m^{6}A peaks as background (Figure S8A), suggesting that other specific regulators may recruit methyltransferase locally as indirect effects of *SRSF7* knockdown.

To understand why only a small part of SRSF7-binding peaks can affect m^{6}A methylation, we performed motif enrichment analysis for the SRSF7 iCLIP-seq peaks that overlapped with the 911 SRSF7 directly regulated m^{6}A peaks using all SRSF7 iCLIP-seq peaks as background. As shown in Figure S8B, there are 10 motifs significantly ($P < 1 \times 10^{-4}$) enriched in the SRSF7 iCLIP-seq peaks that affect m^{6}A. The most significantly enriched motifs are m^{6}A motifs, suggesting that the existence of m^{6}A motif near SRSF7-binding sites is necessary for SRSF7 to promote the m^{6}A methylation. This is consistent with our finding that tethering SRSF7 promotes the m^{6}A methylation of a nearby m^{6}A motif but not the disruptive m^{6}A motif with mutation right beside the m^{6}A site (Figure 2K). The enrichment of non-m^{6}A motifs suggests that the regulatory role of SRSF7 on m^{6}A may be modulated by other factors colocalized with SRSF7 (Figure S8B). On the other hand, it has been reported that protein modifications of SRSF7 are important for SRSF7 to play different roles on RNA metabolisms. For example, phosphorylated SRSF7 affects RNA splicing, while dephosphorylated SRSF7 promotes nuclear exportation of RNAs [3]. In this study, we found that SRSF7 regulates alternative splicing events and APA events occurring independently with m^{6}A peaks (Figure 7A–D), suggesting that there is also a comparable fraction of SRSF7-binding sites required for proper alternative splicing and APA other than m^{6}A methylation in GBM cells, and probably more sites take charge for nuclear exportation of RNAs. In addition, not all RBP-binding sites reported by CLIP-seq are functional because the binding may not be strong enough. Considering that there are also a small portion of SRSF7-binding sites that can affect alternative splicing, the number of m^{6}A-regulating SRSF7-binding sites looks reasonable for specific regulators that do not affects the nuclear speckle localization of methyltransferases (Figure S6H and I).

m^{6}A has been reported to play important roles in cancer development [52–55]. Global disruption of m^{6}A by METTL3 depletion has been found to affect tumor growth, invasion, migration, metastasis, chemoresistance, and so on, in a variety of cancers via regulating the m^{6}A of diverse downstream genes [16,18,70]. GBM is the most prevalent and malignant primary brain tumor, and characterized by rapid tumor growth, highly diffuse infiltration, and chemoresistance, as well as poor prognosis, with the median survival of GBM patients less than 15 months after diagnosis [71]. Cui et al. reported that METTL3 functions as a tumor suppressor to inhibit the growth and self-renewal of GBM stem cells [51]. Consistently, Zhang et al. reported that demethylase ALKBH5 is essential for GBM stem cell self-renewal and proliferation [50]. Based on different GBM cell lines used by Cui et al. and Zhang et al., another two groups reported that METTL3 is highly expressed in GBM cells and plays oncogenic roles in promoting the growth, migration, invasion, and radiotherapy resistance in GBM cells [48,49]. These diverse and somewhat conflicting roles of m^{6}A in GBM are mediated by different m^{6}A targets, suggesting that the roles of m^{6}A in GBM depend on the contexts and specific downstream m^{6}A targets. Since different m^{6}A sites may direct different roles of m^{6}A in GBM, targeting more specific m^{6}A sites may be a promising direction in GBM therapy. It is possible that the abnormal expression of m^{6}A *trans*-regulators, which guide the deposition of METTL3 on highly specific downstream targets, causes dysregulation of more specific m^{6}A sites with converged functions in GBM. On the other hand, the gene expression levels of *SRSF7* and *METTL3* are positively correlated in majority of cancer types of The Cancer Genome Atlas (TCGA) (Figure S9), and both *SRSF7* and *PBK* show significantly higher gene expression in multiple cancer types (Figures S10 and S11), suggesting that the regulatory role of SRSF7 on m^{6}A may also contribute the tumorigenicities of other cancers. Elucidating the m^{6}A regulators that underlie this process may provide diverse drug targets with much fewer side effects for a variety of cancers.

Materials and methods

Cell culture and reagents

HEK293T cells, HNAs (ScienCell), and glioma cell lines, including U87MG, LN229, A172, LN18, LN428, LN443, SNB19, T98G, U118MG, U251, and U138MG, were cultured in Gibco dulbecco's modified eagle medium (DMEM) containing 10% fetal bovine serum (FBS) at 37 °C in a humidified incubator with 5% CO_2. All cells used in this study were confirmed mycoplasma-free.

Tissue specimen collection

Both paraffin-embedded normal brain and glioma specimens were collected from glioma patients diagnosed from 2001 to 2006 at the First Affiliated Hospital of Sun Yat-sen University, Guangzhou, China.

Construction of plasmids, siRNAs, and stable cell lines

For overexpression, the FL CDS region of *SRSF7* was subcloned into the pSin-EF2 lentiviral system. For gene silencing, short-hairpin RNA (shRNA) oligos were constructed into pLKO.1 vector. The pSin-EF2-SRSF7 and pLKO.1-shSRSF7#1/2 plasmids were transfected into HEK293T cells with packing plasmids pMD2.G and psPAX2 to produce lentiviruses. Glioma cell lines were separately infected with these lentiviruses for 48 h, and later treated with puromycin for 7 days at a concentration of 0.5 μg/ml to construct stable cell lines. In addition, for the plasmids used in Co-IP, the Flag-tagged FL CDS regions of *SRSF7*, *METTL3*, and *WTAP* were subcloned into pcDNA3.1 vector, respectively, and then were transfected into U87MG cells with Lipofectamine 3000 (Catalog No. L3000075, ThermoFisher Scientific, Waltham, MA). For rescue assays, the FL CDS region of *SRSF7* with synonymous point mutations (by mutating AGAACTG TATGGATTGCGAGA to AGAACCGTGTG GATCGCGCGC) was inserted into pLVX-IRES-neo plasmid to avoid being targeting by shRNAs of *SRSF7*. The *PBK* overexpression plasmid was constructed by inserting the FL CDS region of the major isoform of *PBK* (RefSeq ID: NM_018492) into pCDH-CMV-MCS-EF1-Puro vector. The two synonymous point mutations, which do not change amino acids, were introduced in to *PBK* at m^{6}A sites 1041 and 1071 by mutating A to G.

Moreover, three *SRSF7* siRNAs, two *METTL3* siRNAs, two *WTAP* siRNAs, and two *IGF2BP2* siRNAs were purchased from RiboBio, China. All the sequences of siRNA oligos, PCR primers, and shRNA oligos are listed in Table S3.

Co-IP and Western blot

Cells were lysed with 1× E1A lysis buffer [250 mM NaCl, 50 mM N-2-hydroxyethylpiperazine-N-2-ethane sulfonic acid (HEPES), 0.1% NP-40, 5 mM EDTA, pH 7.5] supplemented with 1 mM phenylmethylsulfonyl fluoride (PMSF) and 1× protease inhibitor cocktail (Catalog No. P8340, Sigma, Darmstadt, Germany). The lysate was sonicated on ice and centrifuged at 4 °C for 15 min, and then immunoprecipitated with Anti-Flag beads (Catalog No. M8823, Sigma, Darmstadt, Germany) overnight. The immunoprecipitates were washed five times with 1× E1A lysis buffer and samples were boiled with 2× sodium dodecyl sulphate (SDS) loading buffer at 100 °C for 10 min and ready for Western blot.

Proteins were separated by SDS-polyacrylamide gel electrophoresis, transferred onto hydrophilic polyvinylidene fluoride (PVDF) membranes, blocked with 5% nonfat milk, and then probed with the following antibodies: anti-METTL3 (1:1000; Catalog No. 15073-1-AP, Proteintech, Wuhan, China), anti-METTL14 (1:1000; Catalog No. HPA038002, Sigma), anti-WTAP (1:1000; Catalog No. ab195380, Abcam, Cambridge, UK), anti-SRSF7 (1:1000; Catalog No. 11044-1-AP, Proteintech), anti-PBK (1:1000; Catalog No. 16110-1-AP, Proteintech), anti-α-tubulin (1:1000; Catalog No. 66031, Proteintech), and anti-Flag (1:1000; Catalog No. F3615, Sigma).

3D-SIM

For protein colocalization between SRSF7 and the methyltransferase complex, 1.5×10^3 of SRSF7 (Flag-tagged)-overexpressed U87MG cels were seeded into a chambered cover glass (Lab-Tek; Catalog No. 155411, ThermoFisher Scientific), and the immunofluorescence staining was performed with Immunofluorescence Application Solutions Kit (Catalog No. 12727, Cell Signaling Technology, Danvers, MA) according to the manufacturer's protocol. In brief, cells were fixed with 4% formaldehyde the next day, permeabilized with 0.2% Triton X-100 and blocked with Immunofluorescence Blocking Buffer for 1 h, and then incubated with primary antibodies [anti-METTL3 (1:1000; Catalog No. ab195352, Abcam), anti-METTL14 (1:200; Catalog No. HPA038002, Sigma), anti-WTAP (1:500; Catalog No. ab195380, Abcam), and anti-Flag (1:200; Catalog No. F3165, Sigma)] at 4 °C overnight. The samples were washed three times with 1× Wash Buffer the next day and probed with Alexa 488- and 647- conjugated secondary antibodies (ThermoFisher Scientific). The images were taken by using 100× oil-immersion objective of A1R N-SIM N-STORM microscope (Nikon). All SIM images were cropped and processed with network and information systems (NIS) Elements software.

For nuclear speckle localization of methyltransferases, the U87MG cells were transfected with *SRSF7* siRNA and negative control siRNA for 48 h, respectively, and the immunofluorescence staining was performed as described above, and incubated with primary antibodies [anti-METTL3 (1:1000; Catalog No. ab195352, Abcam), anti-METTL14 (1:200; Catalog No. HPA038002, Sigma), anti-WTAP (1:500; Catalog No. ab195380, Abcam), and anti-SC35 (1:200; Catalog No. ab11826, Abcam)] at 4 °C overnight.

RNA isolation and qRT-PCR

Total RNA was extracted using Trizol reagent (Catalog No. 15596018, ThermoFisher Scientific). 1 μg RNA was reverse transcribed using GoScript Reverse Transcription Mix (Catalog No. A2790, Promega, Fitchburg, WI) according to the manufacturer's protocol. qRT-PCR was performed using ChamQ SYBR qPCR master Mix (Catalog No. Q311-02, Vazyme, Nanjing, China). Primers used in the qRT-PCR are listed in Table S3.

m^6A-seq

Low input m^6A-seq was performed by using a protocol reported by Zeng et al. [72] with some modifications. Briefly, total RNA was isolated from control U87MG cells and U87MG cells transfected with si-*SRSF7*-1 for 48 h. A total of 8–10 μg total RNA was fragmented using the 10× RNA Fragmentation Buffer (100 mM Tris-HCl, 100 mM $ZnCl_2$). The fragmented RNA was immunoprecipitated with 5 μg anti-m^6A antibody (Catalog No. 202003, Synaptic Systems, Goettingen, Germany), 30 μl protein-A/G magnetic beads (Catalog No. 10002D/10004D, ThermoFisher Scientific), 200 U RNase inhibitor (Catalog No. N2611, Promega) in 500 μl IP buffer (150 mM NaCl, 10 mM Tris-HCl at pH 7.5, 0.1% IGEPAL CA-630 in nuclease free H_2O) at 4 °C for 6 h. The samples were then washed twice using IP buffer and eluted by competition with m^6A sodium salt (Catalog No. M2780, Sigma). For high-throughput sequencing, both input and IP samples were used for library construction with the SMARTer Stranded Total RNA-seq Kit v2 (Catalog No. 634413, Takara, Mountain View, CA), and sequenced by Illumina HiSeq X Ten to produce 150-bp paired-end reads.

iCLIP-seq

iCLIP was performed based on a protocol described by Yao et al. [73] with minor modifications. Briefly, U87MG cells were UV-crosslinked with 400 mJ/cm^2 at 254 nm and lysed with 500 μl cell lysis buffer (50 mM Tris-HCl at pH 7.4, 100 mM NaCl, 1% NP-40, 0.1% SDS, 0.5% sodium deoxycholate), followed by immunoprecipitation with 10 μg anti-SRSF7 antibody (Catalog No. RN079PW, MBL, Tokyo, Japan) and 100 μl protein A beads (Catalog No. 10002D, ThermoFisher Scientific) at 4 °C overnight and washing as described. After dephosphorylation of the 5′ ends of RNAs, linker ligation, RNA 5′ end labeling, SDS-PAGE, and membrane transfer, the RNA was harvested and reverse transcribed by Superscript III (Catalog No. 18080044, ThermoFisher Scientific). The cDNA libraries were generated as protocol described and sequenced by Illumina NovaSeq 6000 to produce 50-bp single-end reads.

Validation of differentially methylated m^6A sites

We used SELECT method to validate the differentially methylated m^6A sites according to the described protocol [45]. Briefly, total RNA was mixed with 40 nM up/down primer and 5 μM dNTP in 17 μl 1× CutSmart buffer (Catalog No. B7204S, NEB, Ipswich, MA). The mixture was annealed at a temperature gradient: 90 °C, 1 min; 80 °C, 1 min; 70 °C, 1 min; 60 °C, 1 min; 50 °C, 1 min; and 40 °C, 6 min. Then 0.5 U SplintR ligase (Catalog No. M0375S, NEB), 0.01 U *Bst* 2.0 DNA polymerase (Catalog No. M0537S, NEB), and 10 nM ATP (Catalog No. P0756L, NEB) was added to a final volume of 20 μl and incubated at 40 °C for 20 min, denatured at 80 °C for 20 min, followed by qPCR. The cycle threshold (Ct) values of SELECT samples at indicated m^6A sites were normalized to the Ct values of corresponding non-modification control sites. Primers used in the SELECT assay are listed in Table S3.

Tethering assay

The FL CDS regions of *SRSF7* and *METTL3* fused with a lambda peptide sequence were cloned into pcDNA3.1, the plasmid with only a lambda peptide sequence was used as negative control. The reporter plasmid (pmirGLO-dual luciferase-5BoxB) and the effector plasmids (λ, SRSF7-λ, and METTL3-λ) was transfected in U87MG cells at the ratio 1:9. The transfected cells were harvested at 24 h after transfection, and the total RNA was extracted with Trizol reagent (Catalog No. 15596018, ThermoFisher Scientific) and subjected to SELCET analysis [45]. Primers designed for plasmid construction and SELECT are listed in Table S3.

RIP-qPCR analysis

Cells were harvested and lysed in NP-40 lysis buffer (20 mM Tris-HCl at pH 7.5, 100 mM KCl, 5 mM $MgCl_2$, and 0.5% NP-40), and then cell lysates were immunoprecipitated with 10 μg anti-METTL3 (Catalog No. 15073-1-AP, Proteintech), or anti-METTL14 (Catalog No. 26158-1-AP, Proteintech), or anti-WTAP (Catalog No. ab195380, Abcam), and 100 μl protein G beads (Catalog No. 10004D, ThermoFisher Scientific) at 4 °C overnight, followed by DNase I treatment and proteinase K treatment. The bound RNAs were extracted by Trizol reagent, reverse transcribed into cDNAs, and subjected to qPCR analysis.

Cell proliferation assay, colony formation assay, migration assay, and sphere formation assay

For cell growth curve, 1×10^3 cells were seeded into 96-well plates and stained with MTT (Catalog No. M2003, Sigma-Aldrich) dye, and measured the absorbance at 570 nm. Colony formation assays were performed by seeding cells (1×10^3) into 12-well plates, cultured for 7 days, and then fixed with methanol and stained with crystal violet.

For EdU assays, 2×10^4 cells were seeded into 48-well plates, and EdU assays were performed using the EdU Cell Proliferation Assay Kit (Catalog No. C10310-1, RiboBio, Guangzhou, China). Cell migration assays were performed by seeding 2×10^4 cells into 24-well transwell polycarbonate membrane cell culture inserts and stained with crystal violet.

For sphere formation assays, 3×10^3 cells were seeded into Ultra-Low Attachment Multiple Well Plate, and cultured in the stem cell culture condition for 7 days.

Intracranial xenograft

Five-week-old female BALB/c nude mice were obtained from Beijing Vital River (Beijing, China) and divided into two groups (*SRSF7*-knockdown and control, $n = 6$ per group). Each mouse was injected with 5×10^5 U87MG cells which express luciferase in the right cerebrum. Tumor growth was monitored by Bioluminescent imaging every week.

RNA stability assay

Cells were treated with 5 μg/ml actinomycin D (Catalog No. A9415, Sigma) and collected at 0 h, 3 h, 6 h, and 9 h after treatment. The total RNA was isolated, reverse transcribed into cDNA, and subjected to qPCR analysis.

m^{6}A-seq data analysis

The first end of the raw paired-end reads of the m^{6}A-seq was trimmed to 50 bp from the 3′ end for m^{6}A peak calling and downstream analyses. We mapped the reads to hg19 human genome using HISTA2 (v2.1.0) [74]. The m^{6}A peaks were identified according to the methods as described in our previous studies [15,39], which was modified from the method published by Dominissini and his colleagues [12]. We created 100-bp sliding windows with 50-bp overlap along the longest isoforms of each Ensembl annotated gene and calculated the reads per kilobase of transcript per million mapped reads (RPKM) for each window for IP and input, respectively. For each window, the ratio of RPKM + 1 between IP and input was calculated as the intensity. The winscore of each window was then calculated as the ratio of intensities between this window and the median of all windows in the same gene. Windows with RPKM > 10 in the IP and winscore (enrichment score) > 2 were defined as the enriched windows in each sample. The m^{6}A peaks were defined as the enriched windows with winscores greater than neighboring windows. The overlapping or just neighboring peaks of the two biological replicates were merged into larger windows, and the 100-bp regions in the middle of the merged peaks were considered as the common peaks, which were further filtered by requiring winscore > 2 in both replicates. The distributions of m^{6}A peaks along 30 bins of mRNA were calculated as we have previously described [15].

The m^{6}A ratio, which quantifies m^{6}A peaks, of each m^{6}A peak was calculated as the ratio of peak RPKM between IP and input. To calculate the fold change of m^{6}A ratios upon *SRSF7* knockdown, we first took the union of the m^{6}A peaks of all samples. The union peaks of two replicates were merged, centralized, and filtered to obtain a set of 100-bp peak regions in the same way as above described for obtaining common peaks. To avoid using the unreliable m^{6}A ratios due to tiny denominators, we filtered out the peaks with input window RPKM < 5 at least one sample or m^{6}A ratio < 0.1 in any control samples. Then the m^{6}A peaks with fold change of m^{6}A ratios upon *SRSF7* knockdown > 1.5 or < 2/3 were determined as the up-regulated or down-regulated m^{6}A peaks. The data were visualized using the Integrative Genomics Viewer (IGV) tool [75], the biological replicates were merged, and the average read coverages were used for visualization. StringTie (v1.3.4d) [76] was used to calculate the transcripts per million (TPMs) of Ensembl annotated genes using the input libraries. We filtered out the genes with mean TPM < 1 in control samples to avoid using unreliable fold change of TPMs due to tiny denominators. Differentially expressed genes were determined using DESeq2 [77] according to the read counts of genes calculated by HTSeq [78]. The genes with false discovery rate (FDR) < 0.05 and mean counts per million (CPM) > 100 were determined as the differentially expressed genes. GO analysis was performed using DAVID [79] with all expressed genes (TPM > 1) as background. The GSEA was performed using GSEA (v2.2.2.0) [80] based on the predefined gene sets from the Molecular Signatures Database (MSigDB v5.0) [80].

Analysis of the clinical data of glioma patients

The gene expression, mutation, and clinical data of glioma patients were downloaded from CGGA database (http://www.cgga.org.cn/) [40]. We used the Cox Regression to examine the correlations between gene expression indexes of the cancer module and patient survival in each cancer type. The gene expression data of all cancer types were downloaded from TCGA (https://tcga-data.nci.nih.gov/).

iCLIP-seq data analysis

We used the CTK to call the peaks from the iCLIP-seq data according to the described data processing procedure of iCLIP-seq [42]. HOMER software [81] was used for motif enrichment analysis with randomly permutated sequences as the background. The overlapping peaks between the peaks of m^{6}A-seq and iCLIP-seq were determined as the peaks with distance < 100 bp using BEDTools [82].

Alternative splicing and APA analyses

We used rMATS [61] to perform the differential alternative splicing analysis using the input RNAs of m^{6}A-seq with FDR < 0.05 as the threshold of significance. The binding enrichment of SRSF7 around splicing events was analyzed using rMAPS2. To test whether the genes with alternative splicing and the genes with SRSF7 directly regulated m^{6}A peaks are significantly overlapped, we only considered all m^{6}A modified genes with rMATS-detected alternative splicing in the Chi-square test. Differential APA analysis was performed using DaPars [63] with FDR < 0.1 as the threshold of significance.

Statistical analysis

Comparisons between two groups were performed using Student's two-tailed *t*-test. Comparisons during more than two groups are performed using ANOVA. Data represent mean ± SEM; *P* value or adjusted *P* value for ANOVA less than 0.05 was considered statistically significant. Survival curves were plotted by the Kaplan–Meier method and compared by the log-rank test. The statistics of bioinformatic analyses were all described along with the results or figures.

Ethical statement

Written informed consents and approvals for all tissue specimens were obtained from the Institutional Research Ethics Committee of Sun Yat-sen University (Approval No. [2020] 322), and all animal experiments were approved by the Institutional Animal Care and Use Committee of Sun Yat-sen University Cancer Center, Guangzhou, China (Approval No. L102012018010T).

Data availability

The raw sequencing reads of m^{6}A-seq and iCLIP-seq have been deposited in the Genome Sequence Archive for Human [83] at the National Genomics Data Center, Beijing Institute of Genomics, Chinese Academy of Sciences / China National Center for Bioinformation (GSA-Human: HRA001166), and are publicly accessible at https://ngdc.cncb.ac.cn/gsa-human/.

Competing interests

The authors have declared no competing interests.

CRediT authorship contribution statement

Yixian Cun: Methodology, Validation, Visualization, Writing – original draft. **Sanqi An:** Software, Formal analysis, Visualization, Writing – original draft. **Haiqing Zheng:** Validation, Visualization, Writing – original draft. **Jing Lan:** Investigation. **Wenfang Chen:** Formal analysis. **Wanjun Luo:** Investigation. **Chengguo Yao:** Investigation. **Xincheng Li:** Investigation. **Xiang Huang:** Resources. **Xiang Sun:** Resources, Funding acquisition. **Zehong Wu:** Formal analysis. **Yameng Hu:** Resources. **Ziwen Li:** Resources. **Shuxia Zhang:** Resources. **Geyan Wu:** Resources. **Meisongzhu Yang:** Resources. **Miaoling Tang:** Resources. **Ruyuan Yu:** Resources. **Xinyi Liao:** Resources. **Guicheng Gao:** Resources. **Wei Zhao:** Resources. **Jinkai Wang:** Conceptualization, Writing – review & editing, Supervision, Project administration, Funding acquisition. **Jun Li:** Conceptualization, Writing – review & editing, Supervision, Project administration, Funding acquisition. All authors have read and approved the final manuscript.

Acknowledgments

We thank Jianzhao Liu for providing the vectors of tethering assay. This work was supported by the National Key R&D Program of China (Grant No. 2018YFA0107200) to JW, the National Natural Science Foundation of China (Grant Nos. 81830082, 82030078, and 81621004 to JL; Grant Nos. 31771446 and 31970594 to JW; Grant No. 32100452 to XS).

Supplementary material

Supplementary data to this article can be found online at https://doi.org/10.1016/j.gpb.2021.11.001.

ORCID

ORCID 0000-0002-3951-942X (Yixian Cun)
ORCID 0000-0002-3177-213X (Sanqi An)
ORCID 0000-0001-7385-3037 (Haiqing Zheng)
ORCID 0000-0001-8313-6795 (Jing Lan)
ORCID 0000-0002-0720-7106 (Wenfang Chen)
ORCID 0000-0001-7388-7552 (Wanjun Luo)
ORCID 0000-0001-9224-0156 (Chengguo Yao)
ORCID 0000-0001-5159-7036 (Xincheng Li)
ORCID 0000-0002-6834-6564 (Xiang Huang)
ORCID 0000-0001-5344-464X (Xiang Sun)
ORCID 0000-0003-4063-6583 (Zehong Wu)
ORCID 0000-0003-0760-4790 (Yameng Hu)
ORCID 0000-0002-2466-9388 (Ziwen Li)
ORCID 0000-0002-1745-4856 (Shuxia Zhang)
ORCID 0000-0001-8034-9592 (Geyan Wu)
ORCID 0000-0001-9725-4573 (Meisongzhu Yang)
ORCID 0000-0001-5844-1640 (Miaoling Tang)
ORCID 0000-0001-6758-4395 (Ruyuan Yu)
ORCID 0000-0002-8190-070X (Xinyi Liao)
ORCID 0000-0002-0904-8153 (Guicheng Gao)

ORCID 0000-0002-0774-2571 (Wei Zhao)
ORCID 0000-0002-2577-7575 (Jinkai Wang)
ORCID 0000-0003-0572-1344 (Jun Li)

References

[1] Howard JM, Sanford JR. The RNAissance family: SR proteins as multifaceted regulators of gene expression. Wiley Interdiscip Rev RNA 2015;6:93–110.
[2] Chen J, Crutchley J, Zhang D, Owzar K, Kastan MB. Identification of a DNA damage-induced alternative splicing pathway that regulates p53 and cellular senescence markers. Cancer Discov 2017;7:766–81.
[3] Huang Y, Yario TA, Steitz JA. A molecular link between SR protein dephosphorylation and mRNA export. Proc Natl Acad Sci U S A 2004;101:9666–70.
[4] Gao L, Wang J, Wang Y, Andreadis A. SR protein 9G8 modulates splicing of tau exon 10 via its proximal downstream intron, a clustering region for frontotemporal dementia mutations. Mol Cell Neurosci 2007;34:48–58.
[5] Müller-McNicoll M, Botti V, de Jesus Domingues AM, Brandl H, Schwich OD, Steiner MC, et al. SR proteins are NXF1 adaptors that link alternative RNA processing to mRNA export. Genes Dev 2016;30:553–66.
[6] Behan FM, Iorio F, Picco G, Gonçalves E, Beaver CM, Migliardi G, et al. Prioritization of cancer therapeutic targets using CRISPR-Cas9 screens. Nature 2019;568:511–6.
[7] Fu Y, Wang Y. SRSF7 knockdown promotes apoptosis of colon and lung cancer cells. Oncol Lett 2018;15:5545–52.
[8] Saijo S, Kuwano Y, Masuda K, Nishikawa T, Rokutan K, Nishida K. Serine/arginine-rich splicing factor 7 regulates p21-dependent growth arrest in colon cancer cells. J Med Invest 2016;63:219–26.
[9] Park WC, Kim HR, Kang DB, Ryu JS, Choi KH, Lee GO, et al. Comparative expression patterns and diagnostic efficacies of SR splicing factors and HNRNPA1 in gastric and colorectal cancer. BMC Cancer 2016;16:358.
[10] Song X, Wan X, Huang T, Zeng C, Sastry N, Wu B, et al. SRSF3-regulated RNA alternative splicing promotes glioblastoma tumorigenicity by affecting multiple cellular processes. Cancer Res 2019;79:5288–301.
[11] Meyer K, Saletore Y, Zumbo P, Elemento O, Mason C, Jaffrey S. Comprehensive analysis of mRNA methylation reveals enrichment in 3′ UTRs and near stop codons. Cell 2012;149:1635–46.
[12] Dominissini D, Moshitch-Moshkovitz S, Schwartz S, Salmon-Divon M, Ungar L, Osenberg S, et al. Topology of the human and mouse m^{6}A RNA methylomes revealed by m6A-seq. Nature 2012;485:201–6.
[13] Desrosiers R, Friderici K, Rottman F. Identification of methylated nucleosides in messenger RNA from Novikoff hepatoma cells. Proc Natl Acad Sci U S A 1974;71:3971–5.
[14] Niu Y, Zhao X, Wu YS, Li MM, Wang XJ, Yang YG. *N*^{6}-methyladenosine (m^{6}A) in RNA: an old modification with a novel epigenetic function. Genomics Proteomics Bioinformatics 2013;11:8–17.
[15] Batista P, Molinie B, Wang J, Qu K, Zhang J, Li L, et al. m^{6}A RNA modification controls cell fate transition in mammalian embryonic stem cells. Cell Stem Cell 2014;15:707–19.
[16] Delaunay S, Frye M. RNA modifications regulating cell fate in cancer. Nat Cell Biol 2019;21:552–9.
[17] Shulman Z, Stern-Ginossar N. The RNA modification *N*^{6}-methyladenosine as a novel regulator of the immune system. Nat Immunol 2020;21:501–12.
[18] Barbieri I, Kouzarides T. Role of RNA modifications in cancer. Nat Rev Cancer 2020;20:303–22.
[19] Livneh I, Moshitch-Moshkovitz S, Amariglio N, Rechavi G, Dominissini D. The m^{6}A epitranscriptome: transcriptome plasticity in brain development and function. Nat Rev Neurosci 2020;21:36–51.
[20] Li Y, Zhang Q, Cui G, Zhao F, Tian X, Sun BF, et al. m^{6}A regulates liver metabolic disorders and hepatogenous diabetes. Genomics Proteomics Bioinformatics 2020;18:371–83.
[21] Zaccara S, Ries RJ, Jaffrey SR. Reading, writing and erasing mRNA methylation. Nat Rev Mol Cell Biol 2019;20:608–24.
[22] Shi H, Wei J, He C. Where, when, and how: context-dependent functions of RNA methylation writers, readers, and erasers. Mol Cell 2019;74:640–50.
[23] Huang J, Yin P. Structural insights into *N*^{6}-methyladenosine (m^{6}A) modification in the transcriptome. Genomics Proteomics Bioinformatics 2018;16:85–98.
[24] Jia G, Fu Y, Zhao X, Dai Q, Zheng G, Yang Y, et al. *N*^{6}-methyladenosine in nuclear RNA is a major substrate of the obesity-associated FTO. Nat Chem Biol 2011;7:885–7.
[25] Zheng G, Dahl J, Niu Y, Fedorcsak P, Huang CM, Li C, et al. ALKBH5 is a mammalian RNA demethylase that impacts RNA metabolism and mouse fertility. Mol Cell 2013;49:18–29.
[26] Liao S, Sun H, Xu C. YTH domain: a family of *N*^{6}-methyladenosine (m^{6}A) readers. Genomics Proteomics Bioinformatics 2018;16:99–107.
[27] Wang X, Lu Z, Gomez A, Hon GC, Yue Y, Han D, et al. *N*^{6}-methyladenosine-dependent regulation of messenger RNA stability. Nature 2014;505:117–20.
[28] Wang X, Zhao B, Roundtree I, Lu Z, Han D, Ma H, et al. *N*^{6}-methyladenosine modulates messenger RNA translation efficiency. Cell 2015;161:1388–99.
[29] Hsu PJ, Zhu Y, Ma H, Guo Y, Shi X, Liu Y, et al. Ythdc2 is an *N*^{6}-methyladenosine binding protein that regulates mammalian spermatogenesis. Cell Res 2017;27:1115–27.
[30] Shi H, Wang X, Lu Z, Zhao BS, Ma H, Hsu PJ, et al. YTHDF3 facilitates translation and decay of *N*^{6}-methyladenosine-modified RNA. Cell Res 2017;27:315–28.
[31] Huang H, Weng H, Sun W, Qin X, Shi H, Wu H, et al. Recognition of RNA *N*^{6}-methyladenosine by IGF2BP proteins enhances mRNA stability and translation. Nat Cell Biol 2018;20:285–95.
[32] Liu J, Dou X, Chen C, Chen C, Liu C, Xu MM, et al. *N*^{6}-methyladenosine of chromosome-associated regulatory RNA regulates chromatin state and transcription. Science 2020;367:580–6.
[33] Li Y, Xia L, Tan K, Ye X, Zuo Z, Li M, et al. *N*^{6}-methyladenosine co-transcriptionally directs the demethylation of histone H3K9me2. Nat Genet 2020;52:870–7.
[34] Yue Y, Liu J, Cui X, Cao J, Luo G, Zhang Z, et al. VIRMA mediates preferential m^{6}A mRNA methylation in 3′ UTR and near stop codon and associates with alternative polyadenylation. Cell Discov 2018;4:10.
[35] Wen J, Lv R, Ma H, Shen H, He C, Wang J, et al. Zc3h13 regulates nuclear RNA m^{6}A methylation and mouse embryonic stem cell self-renewal. Mol Cell 2018;69:1028–38.
[36] Huang H, Weng H, Zhou K, Wu T, Zhao BS, Sun M, et al. Histone H3 trimethylation at lysine 36 guides m^{6}A RNA modification co-transcriptionally. Nature 2019;567:414–9.
[37] Bertero A, Brown S, Madrigal P, Osnato A, Ortmann D, Yiangou L, et al. The SMAD2/3 interactome reveals that TGFβ controls m^{6}A mRNA methylation in pluripotency. Nature 2018;555:256–9.
[38] Lee Y, Rio DC. Mechanisms and regulation of alternative pre-mRNA splicing. Annu Rev Biochem 2015;84:291–323.
[39] An S, Huang W, Huang X, Cun Y, Cheng W, Sun X, et al. Integrative network analysis identifies cell-specific *trans* regulators of m^{6}A. Nucleic Acids Res 2020;48:1715–29.
[40] Zhao Z, Zhang KN, Wang Q, Li G, Zeng F, Zhang Y, et al. Chinese Glioma Genome Atlas (CGGA): a comprehensive resource with functional genomic data from Chinese glioma patients. Genomics Proteomics Bioinformatics 2021;19:1–12.

[41] König J, Zarnack K, Rot G, Curk T, Kayikci M, Zupan B, et al. iCLIP reveals the function of hnRNP particles in splicing at individual nucleotide resolution. Nat Struct Mol Biol 2010;17:909–15.
[42] Shah A, Qian Y, Weyn-Vanhentenryck SM, Zhang C. CLIP Tool Kit (CTK): a flexible and robust pipeline to analyze CLIP sequencing data. Bioinformatics 2017;33:566–7.
[43] Königs V, de Oliveira Freitas Machado C, Arnold B, Blumel N, Solovyeva A, Lobbert S, et al. SRSF7 maintains its homeostasis through the expression of Split-ORFs and nuclear body assembly. Nat Struct Mol Biol 2020;27:260–73.
[44] Behm-Ansmant I, Rehwinkel J, Doerks T, Stark A, Bork P, Izaurralde E. mRNA degradation by miRNAs and GW182 requires both CCR4:NOT deadenylase and DCP1:DCP2 decapping complexes. Genes Dev 2006;20:1885–98.
[45] Xiao Y, Wang Y, Tang Q, Wei L, Zhang X, Jia G. An elongation- and ligation-based qPCR amplification method for the radiolabeling-free detection of locus-specific N^6-methyladenosine modification. Angew Chem Int Ed Engl 2018;57:15995–6000.
[46] Tang Y, Chen K, Song B, Ma J, Wu X, Xu Q, et al. m^6A-Atlas: a comprehensive knowledgebase for unraveling the N^6-methyladenosine (m^6A) epitranscriptome. Nucleic Acids Res 2021;49:D134–43.
[47] Linder B, Grozhik AV, Olarerin-George AO, Meydan C, Mason CE, Jaffrey SR. Single-nucleotide-resolution mapping of m^6A and m^6Am throughout the transcriptome. Nat Methods 2015;12:767–72.
[48] Li F, Yi Y, Miao Y, Long W, Long T, Chen S, et al. N^6-methyladenosine modulates nonsense-mediated mRNA decay in human glioblastoma. Cancer Res 2019;79:5785–98.
[49] Visvanathan A, Patil V, Arora A, Hegde AS, Arivazhagan A, Santosh V, et al. Essential role of METTL3-mediated m^6A modification in glioma stem-like cells maintenance and radioresistance. Oncogene 2018;37:522–33.
[50] Zhang S, Zhao BS, Zhou A, Lin K, Zheng S, Lu Z, et al. m^6A demethylase ALKBH5 maintains tumorigenicity of glioblastoma stem-like cells by sustaining FOXM1 expression and cell proliferation program. Cancer Cell 2017;31:591–606.e6.
[51] Cui Q, Shi H, Ye P, Li L, Qu Q, Sun G, et al. m^6A RNA methylation regulates the self-renewal and tumorigenesis of glioblastoma stem cells. Cell Rep 2017;18:2622–34.
[52] Li Z, Weng H, Su R, Weng X, Zuo Z, Li C, et al. FTO plays an oncogenic role in acute myeloid leukemia as a N^6-methyladenosine RNA demethylase. Cancer Cell 2017;31:127–41.
[53] Liu J, Eckert MA, Harada BT, Liu SM, Lu Z, Yu K, et al. m^6A mRNA methylation regulates AKT activity to promote the proliferation and tumorigenicity of endometrial cancer. Nat Cell Biol 2018;20:1074–83.
[54] Liu T, Wei Q, Jin J, Luo Q, Liu Y, Yang Y, et al. The m^6A reader YTHDF1 promotes ovarian cancer progression via augmenting EIF3C translation. Nucleic Acids Res 2020;48:3816–31.
[55] Paris J, Morgan M, Campos J, Spencer GJ, Shmakova A, Ivanova I, et al. Targeting the RNA m^6A reader YTHDF2 selectively compromises cancer stem cells in acute myeloid leukemia. Cell Stem Cell 2019;25:137–48.e6.
[56] Shih MC, Chen JY, Wu YC, Jan YH, Yang BM, Lu PJ, et al. TOPK/PBK promotes cell migration via modulation of the PI3K/PTEN/AKT pathway and is associated with poor prognosis in lung cancer. Oncogene 2012;31:2389–400.
[57] Ayllón V, O'Connor R. PBK/TOPK promotes tumour cell proliferation through p38 MAPK activity and regulation of the DNA damage response. Oncogene 2007;26:3451–61.
[58] Gao T, Hu Q, Hu X, Lei Q, Feng Z, Yu X, et al. Novel selective TOPK inhibitor SKLB-C05 inhibits colorectal carcinoma growth and metastasis. Cancer Lett 2019;445:11–23.
[59] Joel M, Mughal AA, Grieg Z, Murrell W, Palmero S, Mikkelsen B, et al. Targeting PBK/TOPK decreases growth and survival of glioma initiating cells *in vitro* and attenuates tumor growth *in vivo*. Mol Cancer 2015;14:121.
[60] Yang QX, Zhong S, He L, Jia XJ, Tang H, Cheng ST, et al. PBK overexpression promotes metastasis of hepatocellular carcinoma via activating ETV4-uPAR signaling pathway. Cancer Lett 2019;452:90–102.
[61] Shen S, Park JW, Lu ZX, Lin L, Henry MD, Wu YN, et al. rMATS: robust and flexible detection of differential alternative splicing from replicate RNA-Seq data. Proc Natl Acad Sci U S A 2014;111:E5593–601.
[62] Hwang JY, Jung S, Kook TL, Rouchka EC, Bok J, Park JW. rMAPS2: an update of the RNA map analysis and plotting server for alternative splicing regulation. Nucleic Acids Res 2020;48:W300–6.
[63] Xia Z, Donehower LA, Cooper TA, Neilson JR, Wheeler DA, Wagner EJ, et al. Dynamic analyses of alternative polyadenylation from RNA-seq reveal a 3′-UTR landscape across seven tumour types. Nat Commun 2014;5:5274.
[64] Lindtner S, Zolotukhin AS, Uranishi H, Bear J, Kulkarni V, Smulevitch S, et al. RNA-binding motif protein 15 binds to the RNA transport element RTE and provides a direct link to the NXF1 export pathway. J Biol Chem 2006;281:36915–28.
[65] Xiao W, Adhikari S, Dahal U, Chen YS, Hao YJ, Sun BF, et al. Nuclear m^6A reader YTHDC1 regulates mRNA splicing. Mol Cell 2016;61:507–19.
[66] Kasowitz SD, Ma J, Anderson SJ, Leu NA, Xu Y, Gregory BD, et al. Nuclear m^6A reader YTHDC1 regulates alternative polyadenylation and splicing during mouse oocyte development. PLoS Genet 2018;14:e1007412.
[67] Ke S, Alemu EA, Mertens C, Gantman EC, Fak JJ, Mele A, et al. A majority of m^6A residues are in the last exons, allowing the potential for 3′ UTR regulation. Genes Dev 2015;29:2037–53.
[68] Molinie B, Wang J, Lim KS, Hillebrand R, Lu ZX, Van Wittenberghe N, et al. m^6A-LAIC-seq reveals the census and complexity of the m^6A epitranscriptome. Nat Methods 2016;13:692–8.
[69] Wang J. Integrative analyses of transcriptome data reveal the mechanisms of post-transcriptional regulation. Brief Funct Genomics 2021;20:207–12.
[70] Lian H, Wang QH, Zhu CB, Ma J, Jin WL. Deciphering the epitranscriptome in cancer. Trends Cancer 2018;4:207–21.
[71] Wen PY, Kesari S. Malignant gliomas in adults. N Engl J Med 2008;359:492–507.
[72] Zeng Y, Wang S, Gao S, Soares F, Ahmed M, Guo H, et al. Refined RIP-seq protocol for epitranscriptome analysis with low input materials. PLoS Biol 2018;16:e2006092.
[73] Yao C, Weng L, Shi Y. Global protein–RNA interaction mapping at single nucleotide resolution by iCLIP-seq. Methods Mol Biol 2014;1126:399–410.
[74] Kim D, Paggi JM, Park C, Bennett C, Salzberg SL. Graph-based genome alignment and genotyping with HISAT2 and HISAT-genotype. Nat Biotechnol 2019;37:907–15.
[75] Robinson JT, Thorvaldsdóttir H, Winckler W, Guttman M, Lander ES, Getz G, et al. Integrative genomics viewer. Nat Biotechnol 2011;29:24–6.
[76] Pertea M, Pertea GM, Antonescu CM, Chang TC, Mendell JT, Salzberg SL. StringTie enables improved reconstruction of a transcriptome from RNA-seq reads. Nat Biotechnol 2015;33:290–5.
[77] Love MI, Huber W, Anders S. Moderated estimation of fold change and dispersion for RNA-seq data with DESeq2. Genome Biol 2014;15:550.
[78] Anders S, Pyl PT, Huber W. HTSeq — a Python framework to work with high-throughput sequencing data. Bioinformatics 2015;31:166–9.
[79] Huang da W, Sherman BT, Lempicki RA. Bioinformatics enrichment tools: paths toward the comprehensive functional analysis of large gene lists. Nucleic Acids Res 2009;37:1–13.

[80] Subramanian A, Tamayo P, Mootha VK, Mukherjee S, Ebert BL, Gillette MA, et al. Gene set enrichment analysis: a knowledge-based approach for interpreting genome-wide expression profiles. Proc Natl Acad Sci U S A 2005;102:15545–50.

[81] Heinz S, Benner C, Spann N, Bertolino E, Lin YC, Laslo P, et al. Simple combinations of lineage-determining transcription factors prime *cis*-regulatory elements required for macrophage and B cell identities. Mol Cell 2010;38:576–89.

[82] Quinlan AR, Hall IM. BEDTools: a flexible suite of utilities for comparing genomic features. Bioinformatics 2010;26:841–2.

[83] Chen T, Chen X, Zhang S, Zhu J, Tang B, Wang A, et al. The Genome Sequence Archive Family: toward explosive data growth and diverse data types. Genomics, Proteomics Bioinformatics 2021;19:578–83.